Scientific Research Publishing

International Journal of Geosciences, 2026, 17(3), 183-214
https://www.scirp.org/journal/ijg
ISSN Online: 2156-8367
ISSN Print: 2156-8359

Analysis of the Spatio-Temporal Variability of the Solar Quiet Sq/Sr Ionospheric Currents of the Equatorial EEJ and CEJ/REJ Electrojets by the Ionization Densification Surface

Abdoul Kader Segda[1,2]*, Salfo Kaboré[1,2], Aristide Marie Frédéric Gybre[1,2], Dominique Belemlilga[1,3], Kouadio Olivier Obrou[4], Frédéric Ouattara[1,2]

[1]Laboratory of Analytical Chemistry, Space and Energy Physics (L@CAPSE), Koudougou, Burkina Faso
[2]Department of Physics, Norbert Zongo University (UNZ), Koudougou, Burkina Faso
[3]Department of Physics, Nazi Boni University (UNB), Bobo-Dioulasso, Burkina Faso
[4]Department of Physics, Felix Houphouet-Boigny University (UFHB), Abidjan, Côte d'Ivoire
Email: *ksegda1@gmail.com

How to cite this paper: Segda, A.K., Kaboré, S., Gybre, A.M.F., Belemlilga, D., Obrou, K.O. and Ouattara, F. (2026) Analysis of the Spatio-Temporal Variability of the Solar Quiet Sq/Sr Ionospheric Currents of the Equatorial EEJ and CEJ/REJ Electrojets by the Ionization Densification Surface. *International Journal of Geosciences*, **17**, 183-214.
https://doi.org/10.4236/ijg.2026.173010

Received: January 2, 2026
Accepted: March 27, 2026
Published: March 30, 2026

Abstract

The objective of this article was to analyze the spatiotemporal variability of ionospheric currents, specifically Solar Quiet Sq/Sr, equatorial electrojets (EEJ), and counter-electrojets (CEJ/REJ), across the ionization density surface. The findings, based on the observations of two cities—Singapore (1.28˚N, 103.85˚E) and Bobo-Dioulasso (Guiriko) (11.11˚N, 4.28˚W)—reveal that the power and electron density of the ionization density surface are lower at latitudes closer to the equator than at increasingly distant latitudes. This highlights, on the one hand, the equatorial ionization anomaly and, on the other hand, the very high velocity of electric particles at the equator due to the amplification of the Sq current density observed there. Furthermore, the electric field deduced from the equality of ionospheric power density and the magnitude of the Poynting vector, appearing very weak at the equator, thus confirms the very high electrical conductivity of the Sq currents observed at the equator. Subsequent analysis of the densification surface trajectory shows that the plasma flow movement is twisted and maintains a counterclockwise direction in the Northern Hemisphere and a clockwise direction in the Southern Hemisphere. At latitudes very close to the equator, the overall movement of the two plasma flows indicates, firstly, that the magnetic field cannot be entirely oriented towards the North, and secondly, that the electric field vector is neither horizontal nor vertical, thus suggesting the unlikely existence of an equatorial electrojet. However, by solving a fundamental equation that takes into account mag-

netic declination, and using the Ey component of the electric field, areas with a strong propensity for the formation of EEJs and CEJs will be identified. Thus, for the city of Singapore, EEJ (in the sense of Ey oriented from west to east) will be mainly observed during the hours of vertical drift (3 p.m. and 9 p.m.), while CEJ (in the sense of Ey oriented from east to west) will be observed during the hours of production (3 a.m., 9 a.m. and 12 p.m.) and respectively the reverse for the city of Bobo-Dioulasso. Finally, the analysis shows that equatorial electrojets and counter-electrojets are simply Sq currents amplified by the production factor and therefore of the same nature as Sq.

Keywords

Solar Quiet Sq/Sr, Electroject EEJ, Counter Electroject CEJ/REJ, Conductivity, Current Density, Power Density, Poynting Vector, Production Factor

1. Introduction

As the Earth rotates daily, it is protected from solar wind particles by an envelope called the magnetosphere. This magnetosphere is its own magnetic field, a dipolar field generated within its core. With a magnitude of around ten thousand nanoteslas and a secular variation, this geomagnetic field is called the main magnetic field to distinguish it from other sources known as external or secondary magnetic fields. These external or secondary contributions to the geomagnetic field manifest as fluctuations around the value of the main magnetic field and are observable by ground-based or satellite-borne magnetometers. Some of these fluctuations, occurring daily, are gentle, on the order of a few tens of nanoteslas, while others are sporadic and occasional, on the order of hundreds of nanoteslas. Large-amplitude fluctuations are associated with magnetospheric currents, characteristic of high latitudes, the most prominent manifestations of which are the aurora borealis and australis. Gentle fluctuations, on the other hand, will be associated with ionospheric currents and are characteristic of mid- and low-latitudes. These ionospheric currents will be called "Solar quiet Sq" or "Solar calm Sq" because, according to [1], Sq depends primarily on (local) solar time and is only visible in the absence of disturbances due to the solar wind associated with thunderstorms and substorms, which can easily mask the underlying Sq signals. Finally, according to [2], Sq will be defined as the "average" daily variation of quiet over the five quietest days of a month, while for [3], gentle daily variations will be called "Solar Regulation SR" or "Solar Regulation SR." However, despite this distinction, the term Sq will be used equally well, with a specific mention or clarification, to designate individual variations of days of magnetic quiet as the average of the five quietest days of the month. Demonstrated by George Graham through meticulous observations of a long magnetic needle [4] [5], the atmospheric dynamo effect was proposed as early as 1882 by [6] and further developed by [7] [8] as the driving force

or cause of ionospheric currents Sq. Thus, "According to his dynamo theory, the movement of conductive air (U) through the Earth's magnetic field (B) generates electromotive forces (U × B) which produce electric fields and currents." It was much later, in the 1960s that the simplified theory of the dynamo effect was developed and is abundant in the literature, but its initial developments are summarized in the literature by [9] and [10]. The Sq currents are amplified at the equator, where another controversial ionospheric current, called the equatorial electrojet, first described by [11] in 1951 and flowing eastward, circulates. Controversial because many authors believe that the equatorial electrojet is nothing more than an Sq current, while others believe that they are of a different nature. Besides Sq currents and the equatorial electrojet (EEJ), other ionospheric current systems could also be distinguished, such as currents aligned with interhemispheric field lines and those resulting from the geomagnetic variation induced by lunar tides (L). Finally, regarding Sq currents, according to [1], "despite their small amplitude, studies on Sq have been important for understanding ionospheric electrodynamics [12] [13] and its coupling with the magnetosphere and the lower atmosphere [13]-[15]; for determining a reference level for geomagnetic indices [15]-[17]; for monitoring solar radiation activity [18] [19]; and for estimating terrestrial electrical conductivity [20]-[22]." The ionospheric currents thus presented will also be the subject of reflection or analysis in this article through the ionization densification surface, which has already allowed us to justify the vertical drift and ionization production velocities [23]. To do this, the analysis will be structured essentially after the introduction into three parts: methodology, results and discussion, and after that a conclusion will be presented which will highlight the essence of the reflection and also the possible perspectives.

2. Methodology

The methodology consisted of starting with the motion of the ionization density surface, a notion or concept introduced in [23], to contribute to a better understanding of the vertical drift velocity and ionization production. It emerged that "the ionized part of the ionosphere can be likened to a block of plasma characterized by a rigidity capable of reflecting electromagnetic waves at a given frequency, called the critical frequency foF2, for example. Such a block will have a thickness that increases downwards or towards the depths (due to the prominence of ionizable matter) or decreases upwards at the surface where electromagnetic waves are reflected. This is all the more true because the more powerful the radiation, the more penetrating the solar rays, and the lower the observation altitudes of ionization maxima. Conversely, the less powerful the radiation, the less penetrating the solar rays, and the higher the observation altitudes of ionization maxima." Thus, for example, in the case of less powerful solar radiation, with lower altitudes having less ionization and higher altitudes having more ionization, this would appear as a rise in ionization from these lower layers to reinforce the higher layers. This ionization densification surface will be identified by a position vector whose displacement

$h(t)$ [23] as shown in **Figure 1** below will be proportional to the variation in the power of solar radiation $P_0(t)$ [24] which is the main ionization factor.

$$\begin{cases} h(t) = k\dfrac{\mathrm{d}P_0(t)}{\mathrm{d}t} \\ P_0(t) = 2\sin\left(\dfrac{\pi}{12}t\right)\cos\left(\dfrac{\pi}{6}t\right) \end{cases} \quad (1)$$

$$\rightarrow h(t) = \frac{\pi}{6}k\left[\cos\left(\frac{\pi}{4}t\right) - \sin\left(\frac{\pi}{12}t\right)\sin\left(\frac{\pi}{6}t\right)\right]$$

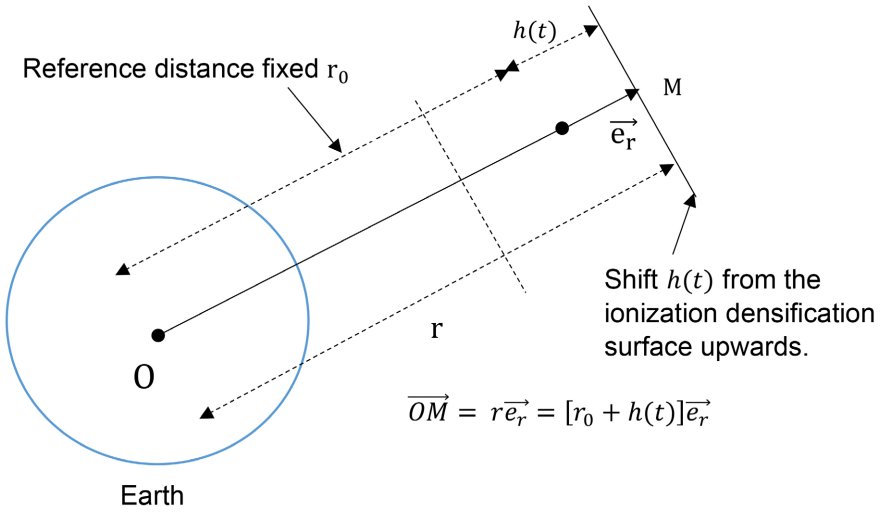

Figure 1. Illustration of the movement of the ionization densification surface in the spherical frame of reference $R_0(\boldsymbol{e}_r, \boldsymbol{e}_\theta, \boldsymbol{e}_\varphi)$ where the position of a point M on the surface is located by (r, θ, φ) called spherical coordinates with reference to the direct orthonormal spherical basis $(\boldsymbol{e}_r, \boldsymbol{e}_\theta, \boldsymbol{e}_\varphi)$.

By differentiating the position vector in a spherical reference frame, we obtain a velocity vector whose component V_{pz}, given by the expression below at a constant latitude λ, is the one that models or simulates the vertical drift velocity or ionization production velocity (**Figure 2** below):

$$\begin{cases} V_{pz}(t) = \dot{h}\sin\lambda \\ V_{pz}(\lambda, k)_{moy} = 36.70\times10^{-2}k\sin\lambda \end{cases} \quad (2)$$

The detailed derivation of the position vector from the spherical reference frame is as follows:

$$\begin{cases} \boldsymbol{OM} = r\boldsymbol{e}_r = \left(r_0 + h(t)\right)\boldsymbol{e}_r \rightarrow \boldsymbol{V}_{M/R_0} = \left.\dfrac{\mathrm{d}\boldsymbol{OM}}{\mathrm{d}t}\right|_{R_0} = \dot{r}\boldsymbol{e}_r + r\dot{\theta}\boldsymbol{e}_\theta + r\dot{\varphi}\sin\theta\boldsymbol{e}_\varphi \\ \dot{r} = \dot{r}_0 + \dot{h}(t), \dot{r}_0 = 0 \rightarrow \dot{r} = \dot{h}(t); \theta = \dfrac{\pi}{2} - \lambda \rightarrow \dot{\theta} = 0 \text{ and } \sin\theta = \cos\lambda \\ \dot{\varphi} = \omega_T = \dfrac{2\pi}{T}, T = 24 \text{ hours} \rightarrow \boldsymbol{V}_{M/R_0} = \left.\dfrac{\mathrm{d}\boldsymbol{OM}}{\mathrm{d}t}\right|_{R_0} = \dot{h}(t)\boldsymbol{e}_r + r\dot{\varphi}\cos\lambda\boldsymbol{e}_\varphi \end{cases}$$

$$\begin{cases} \boldsymbol{V}_{M/R_0} = \dot{h}(t)\boldsymbol{e}_r + r\dot{\varphi}\cos\lambda\boldsymbol{e}_\varphi \to r = r_0 + h(t) \to \\ \boldsymbol{V}_{M/R_0} = r_0\dot{\varphi}\cos\lambda\boldsymbol{e}_\varphi + \dot{h}(t)\boldsymbol{e}_r + h(t)\dot{\varphi}\cos\lambda\boldsymbol{e}_\varphi \\ \boldsymbol{V}_{M/R_0} = \boldsymbol{V}_e + \boldsymbol{V}_r \to \boldsymbol{V}_e = r_0\dot{\varphi}\cos\lambda\boldsymbol{e}_\varphi \text{ and } \boldsymbol{V}_r = \dot{h}(t)\boldsymbol{e}_r + h(t)\dot{\varphi}\cos\lambda\boldsymbol{e}_\varphi \end{cases}$$

$$V_{M/R_1} = \sqrt{\dot{h}(t)^2 + \left[h(t)\dot{\varphi}\cos\lambda\right]^2}$$

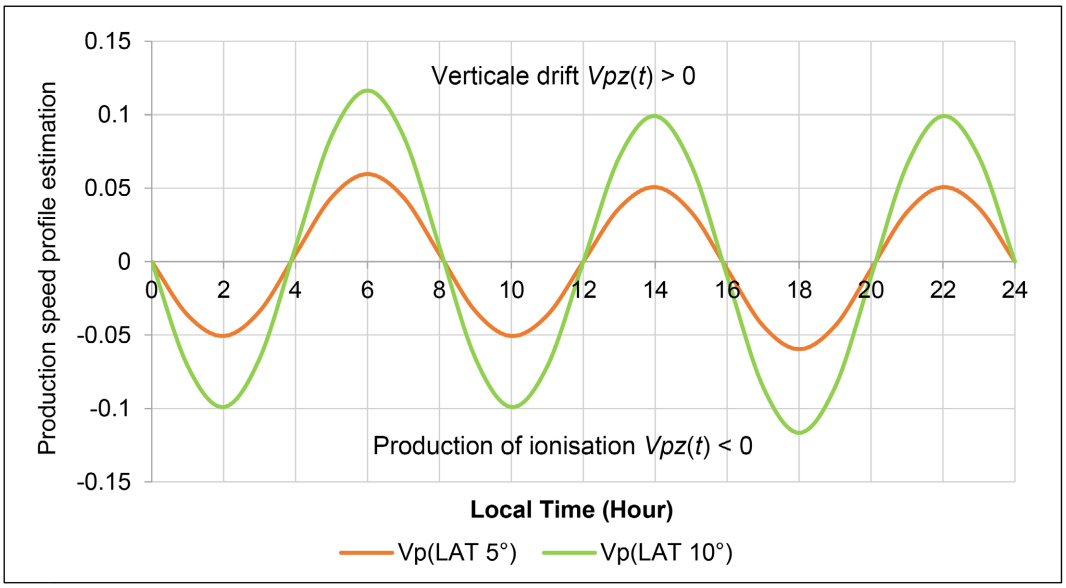

Figure 2. Velocity profiles of production for latitudes of 5˚ and 10˚ following *k*.

Also, knowing the expressions for the basis vectors $\boldsymbol{e}_r$ and $\boldsymbol{e}_\varphi$ depending on the basis vectors $(\boldsymbol{i}, \boldsymbol{j}, \boldsymbol{k})$ from the Cartesian frame of reference, we arrive at the expression for the component V_{pz} of the velocity $\boldsymbol{V}_r$.

$$\begin{pmatrix} \boldsymbol{e}_r \\ \boldsymbol{e}_\theta \\ \boldsymbol{e}_\varphi \end{pmatrix} = \begin{pmatrix} \sin\theta\cos\varphi & \sin\theta\sin\varphi & \cos\theta \\ \cos\theta\cos\varphi & \cos\theta\sin\varphi & -\sin\theta \\ -\sin\varphi & \cos\varphi & 0 \end{pmatrix} \begin{pmatrix} \boldsymbol{i} \\ \boldsymbol{j} \\ \boldsymbol{k} \end{pmatrix}$$

From this expression, we can deduce the average speed over a 24-hour day:

$$\begin{cases} V_{pz}(t) = \dot{h}\cos\theta = \dot{h}\sin\lambda \\ \dot{h}(t) = -\dfrac{\pi^2}{144}k\left[P_0(t) + 8\sin\left(\dfrac{\pi}{4}t\right)\right] \to \left|\dot{h}(t)\right|_{Moy} = 36.70\times10^{-2}k \\ V_{pz}(\lambda,k)_{moy} = 36.70\times10^{-2}k\sin\lambda \end{cases}$$

Knowing the average vertical drift speed and the geographic latitude λ from a city, one can deduce the location of the factor of production. k given by the following expression:

$$k = \frac{V_{pz}(\lambda,k)_{moy}}{36.70\times10^{-2}\sin\lambda}$$

In this article, the study of the densification surface, through the analysis of its motion which also indicates the movement of the plasma flow, will allow us to con-

tribute to a better understanding of ionospheric currents, specifically the Solar Quiet Sq currents, the EEJ electrojet current, and the CEJ/REJ equatorial counter-electrojet current. The ionospheric Sq currents (**Figure 3**) from Yamazaki [25], whose existence was confirmed with the advent of satellites, circulate as vortices in the Northern Hemisphere in a counterclockwise direction and clockwise in the Southern Hemisphere, forming vortices whose foci are respectively far from the equator.

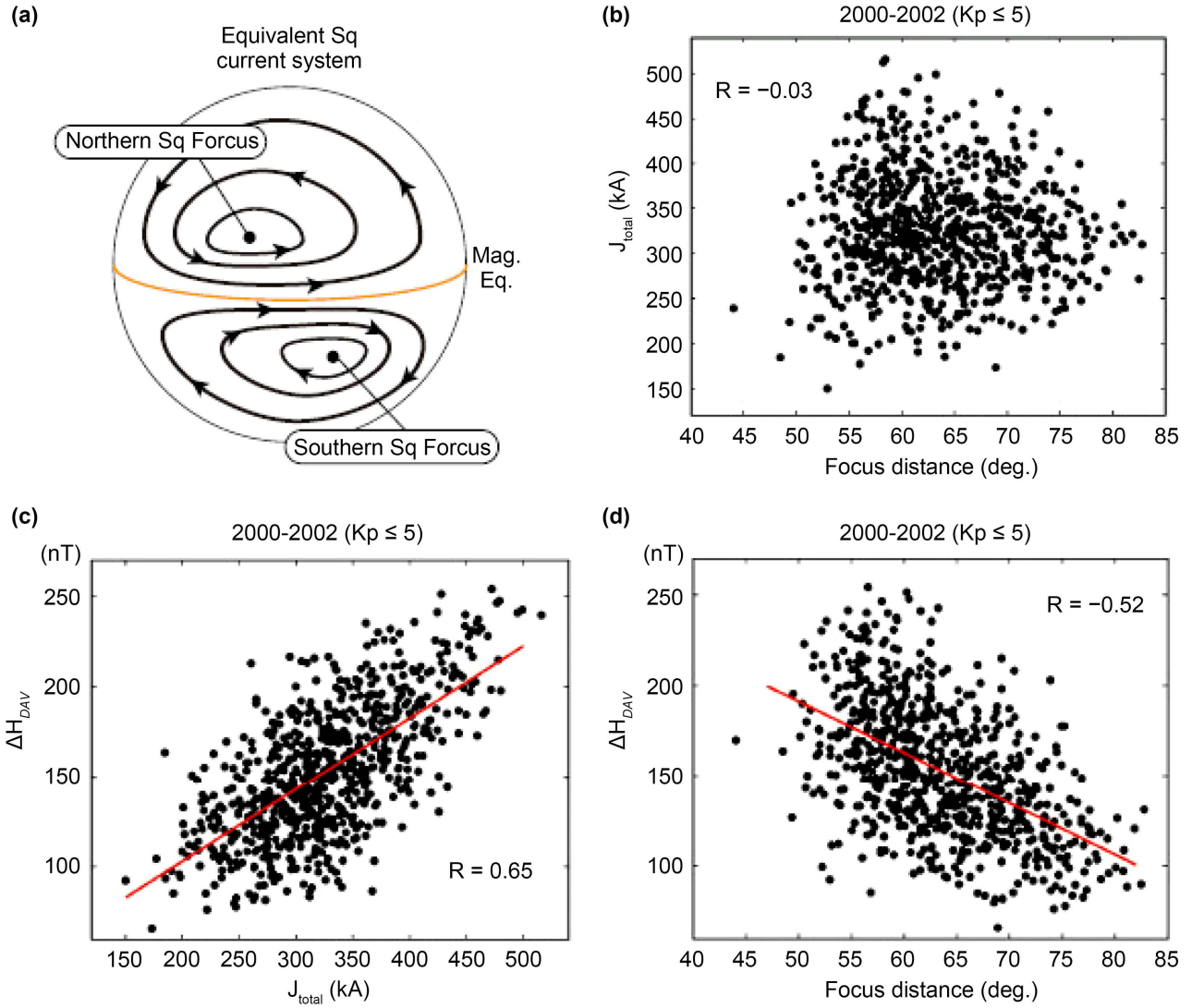

(a) Diagram illustrating the daytime view of the equivalent current system of Sq. (b) Relationship between the total current intensity of Sq and the spherical distance between the north and south foci of Sq. Scatter diagrams: (c) Daily variation of (H) at Davao and J; (d) Daily variation of (H) at Davao and distance to the focus of Sq. from Yamazaki (2011).

Figure 3. Diagram illustrating a view of the equivalent current system Sq [25].

These different currents will join in phase at the equator where their amplifications will be observed, thus leading to the assumption of the existence of the equatorial electroject current EEJ circulating horizontally from West to East in order to provide clarification (**Figure 4**).

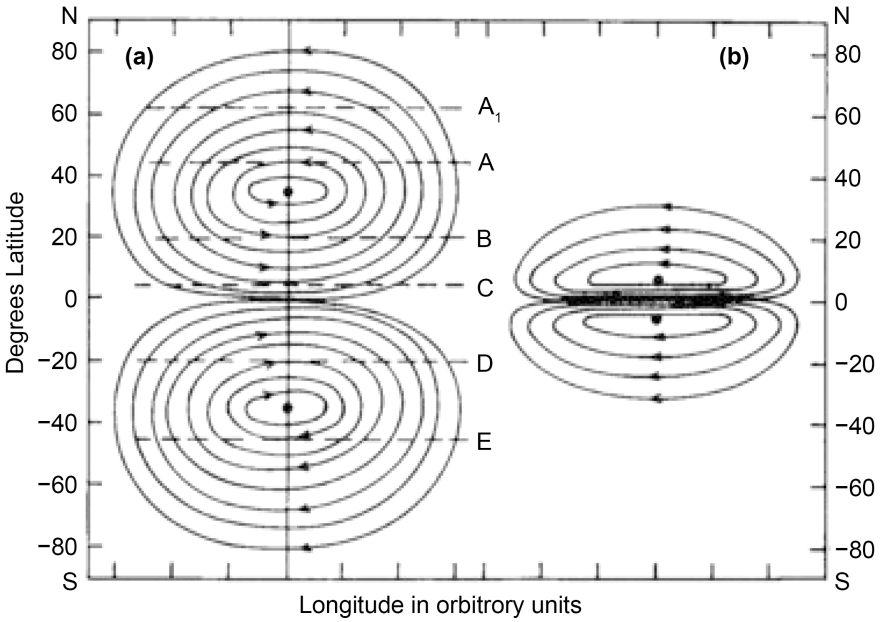

Figure 4. Schematic drawings of (a) global Sq current system and (b) equatorial electrojet current system [26].

Of the same nature as the Sq currents [27] or of a different nature [28], the enhancement of conductivity by the Cowling effect [29] is used to justify the existence of this zonal electric field, denoted E_y, called the equatorial electroject. Indeed, according to Ohm's law derived from the theory of the ionospheric dynamo, it essentially emerges that, just as with the basis vectors $(\boldsymbol{i},\boldsymbol{j},\boldsymbol{k})$ of the Cartesian frame of reference, $(\boldsymbol{e}_\rho,\boldsymbol{e}_\varphi,\boldsymbol{k})$ of the cylindrical frame of reference and $(\boldsymbol{e}_r,\boldsymbol{e}_\theta,\boldsymbol{e}_\varphi)$ of the spherical frame of reference by which one could locate the position of a moving point in space and express its velocity or acceleration, then at any point, the ionosphere will present an electric field vector $\boldsymbol{E}$ three-components by which we can express the ionospheric current density $\boldsymbol{J}$ in this case, that of Sq. Its basic electric field vectors are:

$$\left(\boldsymbol{E}_{//},\boldsymbol{E}_\perp+\boldsymbol{U}\times\boldsymbol{B},\frac{\boldsymbol{B}}{|\boldsymbol{B}|}\times\left(\boldsymbol{E}_\perp+\boldsymbol{U}\times\boldsymbol{B}\right)\right) \tag{3}$$

And where $\boldsymbol{E}_{//},\boldsymbol{E}_\perp$ are electric field vectors that derive from a scalar potential and have zero circulation along a closed contour and $\boldsymbol{U}\times\boldsymbol{B}$ an electromotive field vector derived from a vector potential and with non-zero circulation. Thus, the electric current density vector $\boldsymbol{J}$ can be expressed in terms that give Ohm's law:

$$\begin{cases}\boldsymbol{J}=\sigma_0\boldsymbol{E}_{//}+\sigma_P\left(\boldsymbol{E}_\perp+\boldsymbol{U}\times\boldsymbol{B}\right)+\sigma_H\dfrac{\boldsymbol{B}}{|\boldsymbol{B}|}\times\left(\boldsymbol{E}_\perp+\boldsymbol{U}\times\boldsymbol{B}\right)\\ \sigma(\mathrm{S/m});E(\mathrm{V/m});B(\mathrm{T});J\left(\mathrm{A/m^2}\right)\end{cases} \tag{4}$$

Thus, in this relationship, 1) σ_0 will be called parallel conductivity, giving the current density parallel to the magnetic field $\boldsymbol{B}$. 2) σ_P Pedersen conductivity

gives the current density in the direction of plasma flow and perpendicular to the field $\boldsymbol{B}$. 3) and finally σ_H the Hall conductivity perpendicular to both the magnetic field $\boldsymbol{B}$ and to the electric field $\boldsymbol{E}_\perp$. Of all the conductivities, the conductivity σ_0 is the most important in intensity as shown in Figure 5 below of the model "of the World Data Center for Geomagntism Kyoto" for mid-latitude location 35˚N, 135˚E.

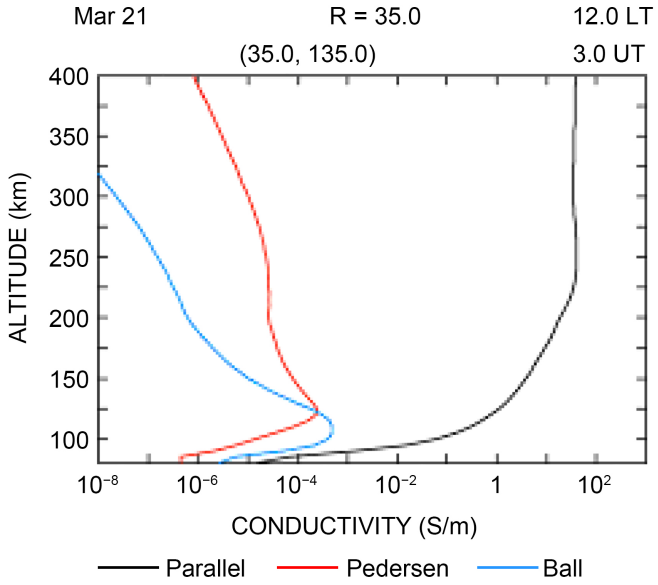

Figure 5. Height profiles of Parallel, Pedersen and Hall conductivities "of the World Data Center for Geomagntism Kyoto" for mid-latitude location 35˚N, 135˚E.

Having described the different conductivities, the equatorial electrojection as shown in Figure 6 below could be explained in these terms: The equatorial electrojection by 1) its electric field $\boldsymbol{E}_y$ or $\boldsymbol{E}_1$ perpendicular to the magnetic field $\boldsymbol{B}$ oriented towards the North will give rise to a Pedersen 1 current of intensity ($J_{P1} = \sigma_{P1} E_1$). 2) This Pedersen current 1 will induce the creation of a downward Hall current 1 of intensity ($J_{H1} = \sigma_{H1} E_1$) in a space charge zone due to the configuration (Figure 5) of the dynamo region in this zone where a polarization field prevails $\boldsymbol{E}_2$. 3) Thus, due to the space charge, the Hall current J_{H1} will be completely inhibited ($J_{H1} = J_{P2}$) by an upward Pedersen current of intensity 2 ($J_{P2} = \sigma_{P2} E_2$) induced by the polarization field E_2. 4) It follows from the creation of the Pedersen current 2 an induction of the creation of a Hall current 2 of intensity ($J_{H2} = \sigma_{H2} E_2$) and oriented from West to East, which would be an addition ($J_{P1} + J_{H2}$) to the Pedersen current 1 thus strengthening the conductivity in this area called Cowling conductivity and given by the relation:

$$\begin{cases} J_{Cowling} = J_{P1} + J_{H2} = \left(\sigma_{P1} + \dfrac{\sigma_{H2} \times \sigma_{H1}}{\sigma_{P2}} \right) E_1 \rightarrow \boldsymbol{J}_{Cowling} = \left(\sigma_P + \dfrac{\sigma_H^2}{\sigma_P} \right) \boldsymbol{E}_1 \\ \sigma_{Cowling} = \sigma_P + \dfrac{\sigma_H^2}{\sigma_P} \end{cases} \quad (5)$$

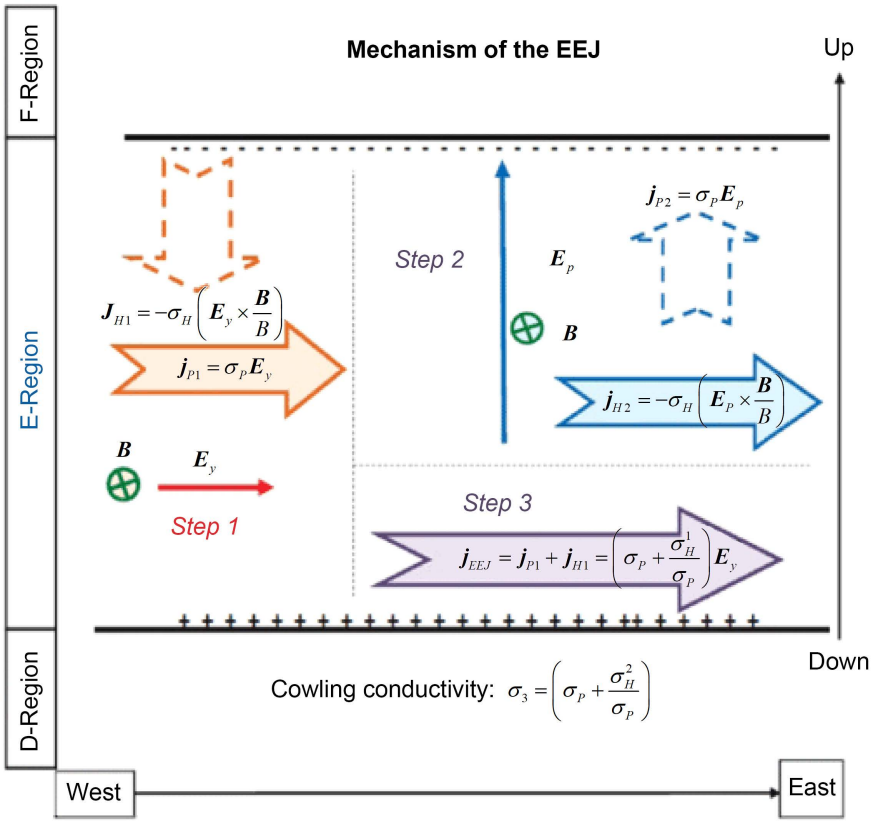

Figure 6. Mechanism for generating the equatorial electrojet, in the plane of the magnetic equator [30].

Counter electrojets (CEJ), on the other hand, are inverted electrojets (REJ), therefore a current system circulating from East to West and most often observed at certain times of day. Several arguments or hypotheses are put forward to clarify this phenomenon. For some, such as 1) [31]-[33], a combination of atmospheric tides could be the cause. 2) For others, such as [34]-[36], it would be more likely a sudden warming of the stratosphere. 3) For others, during periods of geomagnetic activity for [37]-[41], and during the recovery phase of a storm [42] [43]. Finally, 4) thermospheric winds [44] [45] and 5) dust of meteoric origin [46] could also be the cause. Finally, electrojects EEJ and counter electrojects CEJ are used by some, such as [47] [48], to give interpretations to the different variability profiles of critical frequencies foF2.

Thus, for an analysis starting from the densification surface, we will consider that at a constant latitude λ and a longitude φ_0, given the data, the densification surface area will be obtained by the product of the components $x(t)$ and $y(t)$ in Cartesian coordinates given by the following expressions:

$$\begin{cases} x(t) = h\cos\cos\varphi \\ y(t) = h\cos\sin\varphi \end{cases} \rightarrow \varphi(t) = \omega t - \varphi_0 \tag{6}$$

From this surface area, we could calculate the power density " D_p " from Equation (2) below which would allow us to compare the electron density n_e from

latitudes close to the equator to increasingly distant latitudes. This comparison allowed us, on the one hand, to justify the equatorial ionization anomaly, but also to deduce that the factor responsible for the amplification of the current density Sq at the equator is the velocity $V_e(t)$ particles due to the very low electron density.

$$D_p = \frac{kP_0(t)}{S(t)} \text{ and } J = n_e V_e(t) \tag{7}$$

After that, an equality of ionospheric power density with that of light through the magnitude of the Poynting vector allowed us to confirm through Equation (8) that the electrical conductivity was higher at the equator because the electric field was very weak at latitudes close to the equator than at increasingly distant latitudes.

$$J = \sigma \cdot E(t) \tag{8}$$

A representation of the densification surface's movement at each hour showed, firstly, that the movement was counterclockwise and clockwise in the Northern and Southern Hemispheres respectively, and secondly, that their conjunction at the equator was not always in phase.

Also, starting from the hypothesis of a horizontal magnetic field, the expression for the electric field is deduced from the cross product or the intersection of the field $\boldsymbol{B}$ and speed $\boldsymbol{V}$ shows by its components that it is neither horizontal nor vertical.

$$\begin{cases} \boldsymbol{E} = \boldsymbol{B} \times \boldsymbol{V} \\ \boldsymbol{V} = \left(V_{px}, V_{py}, V_{pz}\right), \boldsymbol{B} = \left(B_x, B_y, 0\right) \\ \boldsymbol{E} = B_y V_{pz} \boldsymbol{i} - B_x V_{pz} \boldsymbol{j} + \left(B_x V_{py} - B_y V_{px}\right) \boldsymbol{k} \end{cases} \rightarrow \begin{cases} E_x = B_y V_{pz} \\ E_y = -B_x V_{pz} \\ E_z = B_x V_{py} - B_y V_{px} \end{cases} \tag{9}$$

The same would be true with a non-horizontal or three-component magnetic field, where in such a case the E_y component of $\boldsymbol{E}$ the result would be of the form: $E_y = B_z V_{px} - B_x V_{pz}$.

Finally, the hypothesis of a magnetic field entirely oriented towards the North requires a velocity with components $V_{px} = 0$ and $V_{py} = 0$ which would not be possible because it leads to "$\sin^2 \varphi + \cos^2 \varphi = 0$".

Or also because $\dot{h}$ and h never cancel each other out at the same time as shown in Figure 7 of their temporal variability for example k equal to 1.

From these different hypotheses, we can only deduce that the existence of a horizontal ionospheric current centered at the equator and circulating in a relatively narrow band from west to east at latitudes near the equator, called an equatorial electrojet, seems unlikely. However, it could be formulated in these terms:

1) The conjunction, whether in phase or not, of ionospheric currents already amplified by the production factor in the Northern and Southern hemispheres at the equator leads to an equally amplified ionospheric current whose resulting electric field is neither horizontal nor vertical. However, by the E_y component of the electric field, the moments or periods of high propensity for the formation of electrojets (in the direction of component E_y oriented from West to East), counter-

electrojets (in the direction of component E_y oriented from East to West), and of symmetries and asymmetries in the ionization densification can be identified.

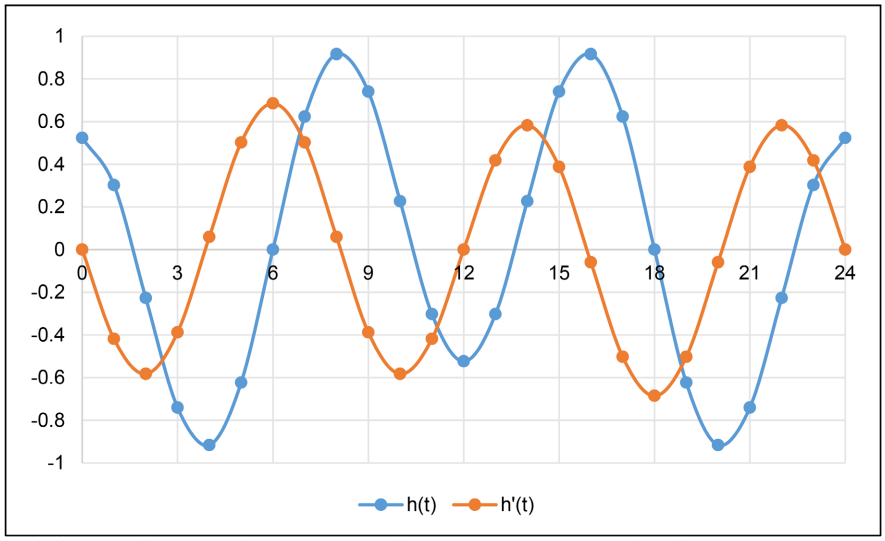

Figure 7. Temporal variability of $h'(t)$ and $h(t)$ for example k equal to 1.

2) From this, electrojects and counter-electrojects will have a propensity to occur at times satisfying the condition " $E_y = -B_x V_{pz}$ " which leads to the solution of the equation below, the details of which are provided in the appendix, with " D " being the angle of magnetic declination.

$$\begin{cases} B \cdot V_{px} \cdot \sin(D) - B \cdot V_{py} \cdot \cos(D) \pm E_z = 0 \\ E_z = \pm\sqrt{E^2 - V_{pz}^2 B^2} \end{cases} \tag{10}$$

3) Also, the sign (EEJ and CEJ) of E_y will be known from $-B_x V_{pz}$ containing also E_z (Annexe). $E_z \geq 0$ during production hours where $V_{pz} \leq 0$ (Due to the downward displacement of the densification surface, resulting in a higher electrical potential in the lower layers than in the upper layers) and $E_z \leq 0$ in the hours of drifting where $V_{pz} \geq 0$ (Due to the upward movement of the densification surface, the electrical potential is therefore higher in the upper layers than in the lower layers).

4) Thus, counter-electrojets will have a strong propensity to occur at the production hours 3 a.m., 9 a.m. and 12 p.m., and electrojets at the vertical drift hours 3 p.m., 9 p.m. and 12 a.m. However, for certain magnetic declination angles, EEJ may occur at 12 p.m. and CEEJ at 9 p.m. and 12 a.m.

5) The symmetries and asymmetries in the ionization density are deduced from the observed movement of the plasma flow at each hemisphere to the resulting overall movement. Finally, the electrical conductivity is deduced from the equality of the current densities given in Equations (7) and (8).

In cases where $B_z \neq 0$ is no-zero the EEJ and CEJ/REJ are always determined from the sign of Ey which would also depend on the angle of inclination " I " of the magnetic field with however the condition given by Equation (11) below (for

details see Annex 2):

$$B^2\cdot\left[\left(V_{pz}\right)^2\cdot\left(\cos D\right)^2+\left(V_{py}\right)^2\cdot\left[\left(\sin I\right)^2+\left(\cos I\cdot\cos D\right)^2\right]\right.$$
$$\left.+\left(V_{px}\right)^2\cdot\left[\left(\sin I\right)^2+\left(\sin I\cdot\cos D\right)^2\right]\right]+B^2\cdot\left[-2\left(V_{pz}\cdot V_{py}\right)\cdot\left(\sin I\right)^2\cdot\cos D\right. \quad (11)$$
$$\left.-\left(V_{pz}\cdot V_{px}\right)\cdot\sin 2I\cdot\cos D-\left(V_{py}\cdot V_{px}\right)\cdot\sin 2I\cdot\left(\cos D\right)^2\right]-E^2=0$$

3. Results

3.1. Average Speed and Production Factor

Figure 8 and Figure 9 below represent, respectively, the variability profiles of the vertical drift velocity of the city of Singapore located at the geographic position Latitude North 1.28˚N and Longitude 103.85˚E and the city of Bobo-Dioulasso Latitude North 11.11˚N and Longitude 4.28˚E. The calculated average of these velocities over the entire day made it possible to determine the production factor *k*.

1) City of Singapore (SGP) (Lat 1.28˚N, Long 103.85˚E)

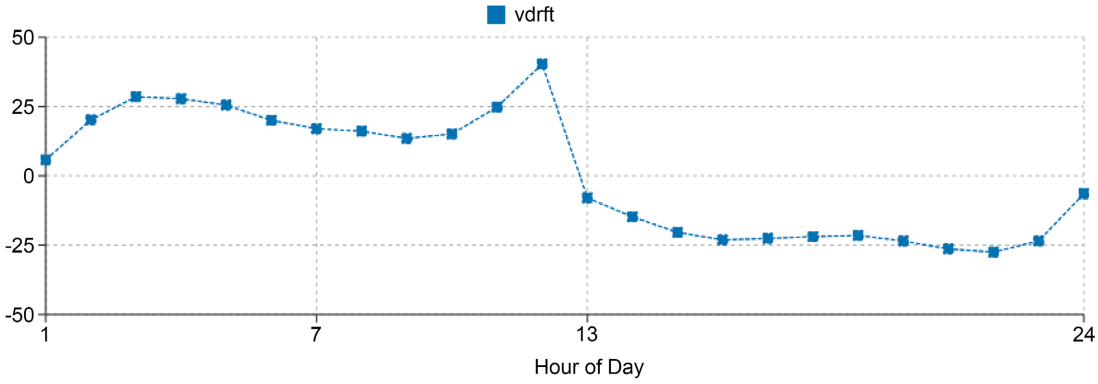

Figure 8. Vertical drift velocity profile for Singapore as of 13/09/2025 using IRI 2020 Average velocity: $V_{moy}=20.59\ \mathrm{m\cdot s^{-1}}$ and Production Factor $k=2511.54\ \mathrm{W\cdot m^{-1}}$.

2) City of Bobo-Dioulasso Guiriko (GKO) (Lat 11.11˚N, Log 4.28˚W)

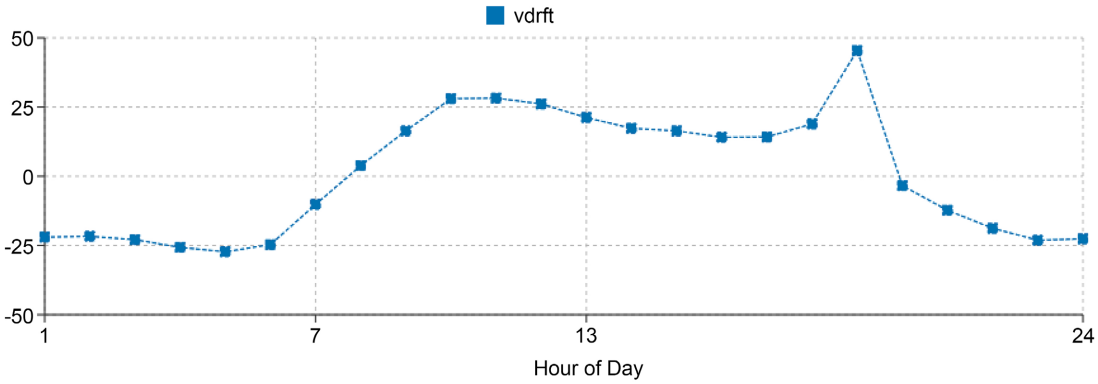

Figure 9. Vertical drift velocity profile Bobo-Dioulasso Guiriko as of 13/09/2025 with IRI 2020 Average velocity: $V_{moy}=20.19\ \mathrm{m\cdot s^{-1}}$ and Production Factor $k=285.72\ \mathrm{W\cdot m^{-1}}$.

3.2. Movement of the Densification Surface

Figure 10 and Figure 11 represent the movement of the densification surface of two cities symmetrical with respect to the equator to show the conjunction or non-conjunction of the plasma near the equator. Figure 10 represents the position of the city of Bobo-Dioulasso located at a northern latitude, and Figure 11 represents another symmetrical geographical position located at a southern latitude.

1) City of Bobo-Dioulasso Guiriko (GKO) (Lat 11.11˚N, Log 4.28˚W)

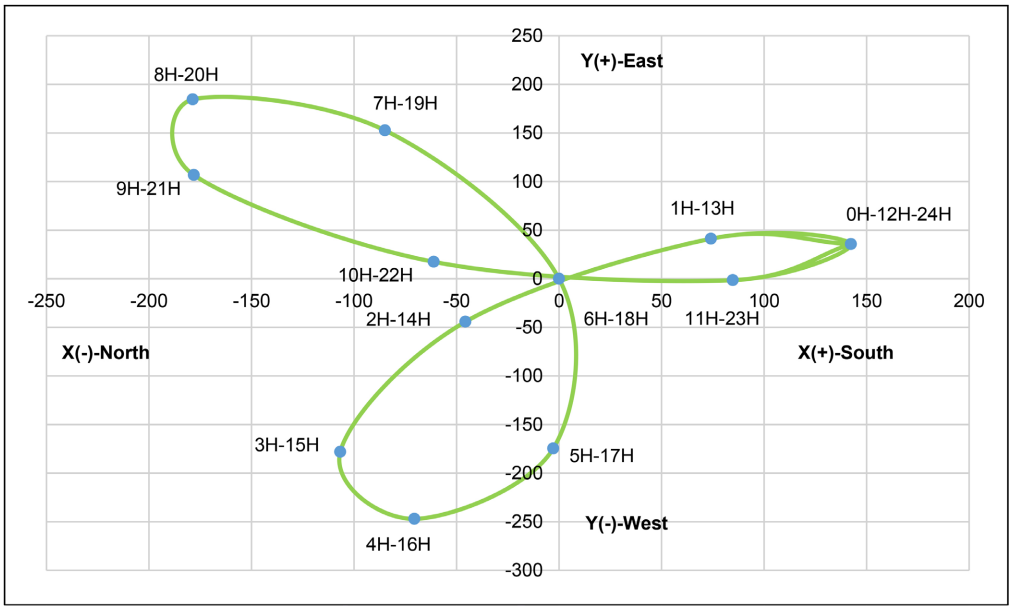

Figure 10. Movement of the ionospheric plasma flux-Bobo-Dioulasso (Lat 11.11˚N, Long 4.28˚W).

2) Latitude 11.11˚S, Longitude 4.28˚W

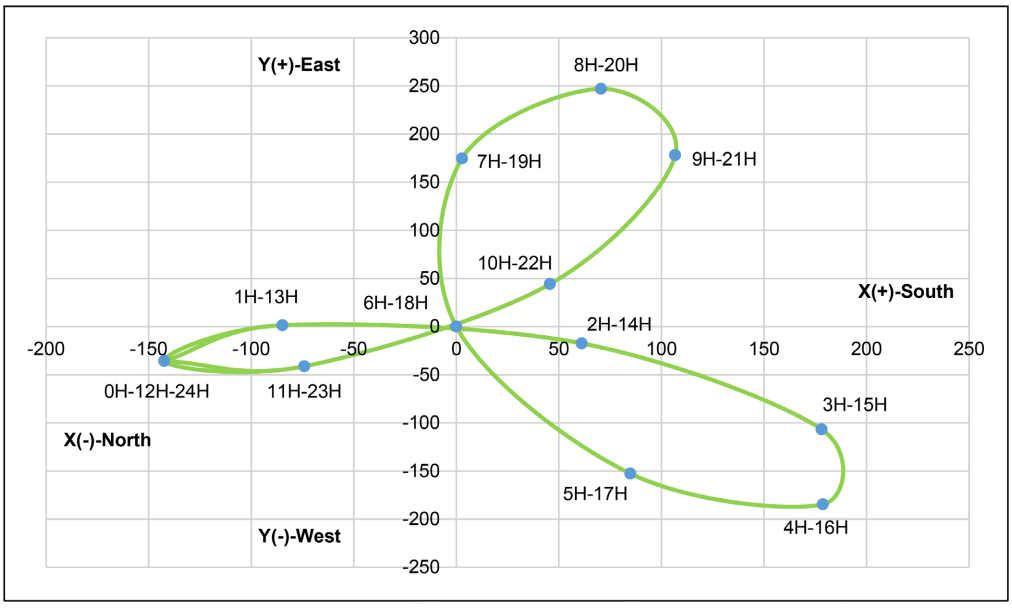

Figure 11. Movement of the ionospheric plasma flux (Lat 11.11˚S, Long 4.28˚W).

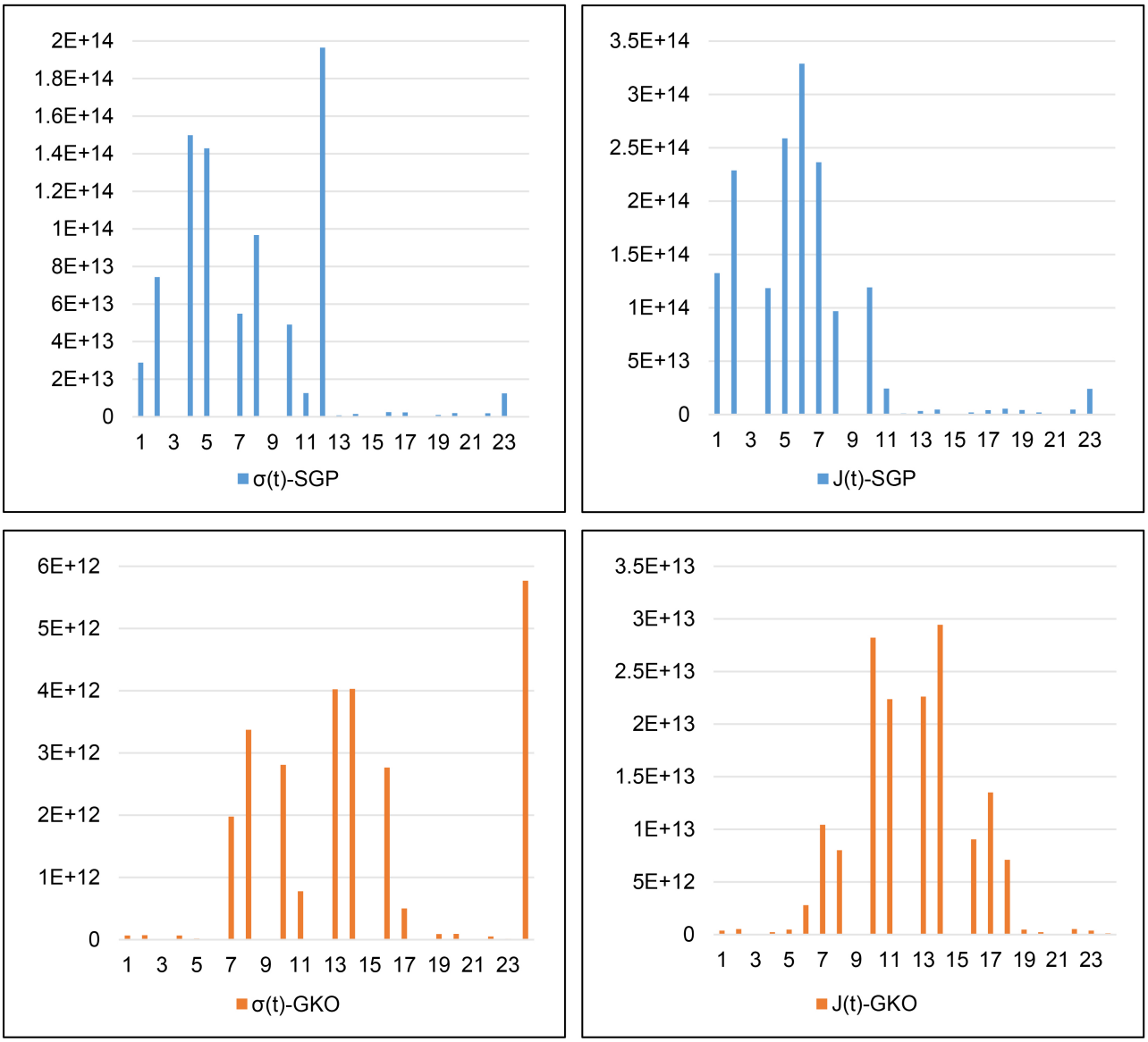

Note: Other results will be used in the discussion section.

Figure 12. Conductivity and electrical density calculated with NmE respectively—Singapore (SGP) (Lat 1.28˚N, Long 103.85˚E) and Bobo-Dioulasso (GKO) (Lat 11.11˚S, Long 4.28˚W).

4. Discussion

4.1. Power Density-Electric Field and Electrical Conductivity

Considering temporal variability $S(t)$ From the ionization densification surface (**Figure 12**) during the day for the city of Singapore (SGP) (Lat 1.28˚N, Long 103.85˚E), considered the closest city to the geographic equator globally, and the city of Bobo-Dioulasso (Guiriko-GKO) (Lat 11.11˚N, Log 4.28˚W) on September 13, 2025, we obtain, using IRI 2020, an average velocity and a production factor for the city of Singapore, respectively. (20.59 m·s^{-1}, k = 2511.54) and for the city of Bobo-Dioulasso (Guiriko) (20.19 m·s^{-1}, k = 285.72).

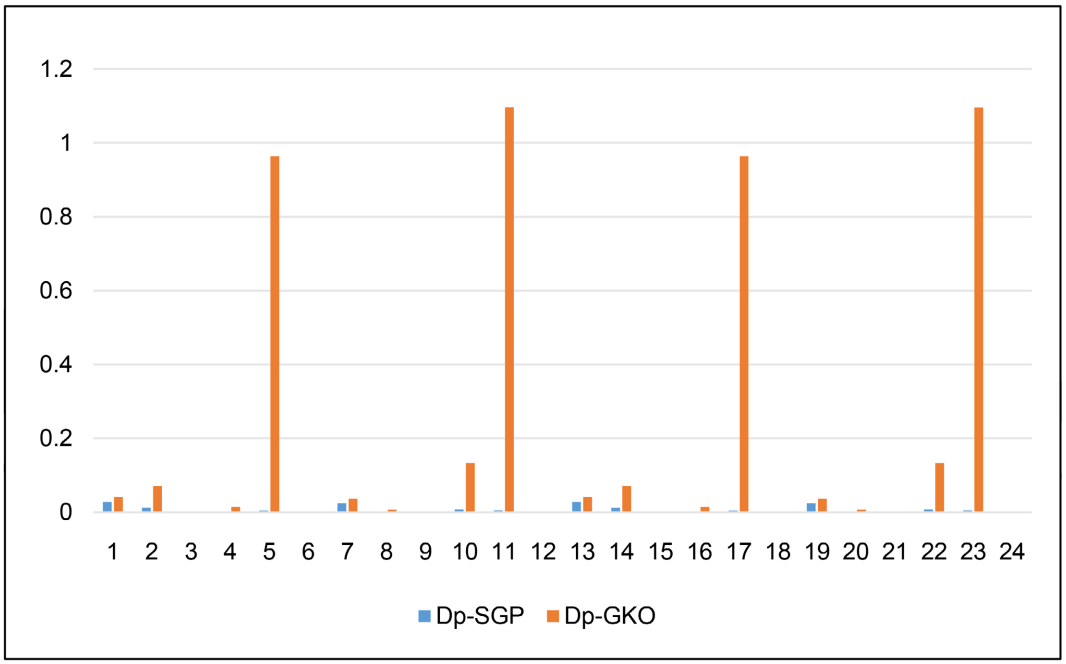

Figure 13. Power density in W/m² city of Singapore and city of Bobo-Dioulasso—6H and 18H are very high values.

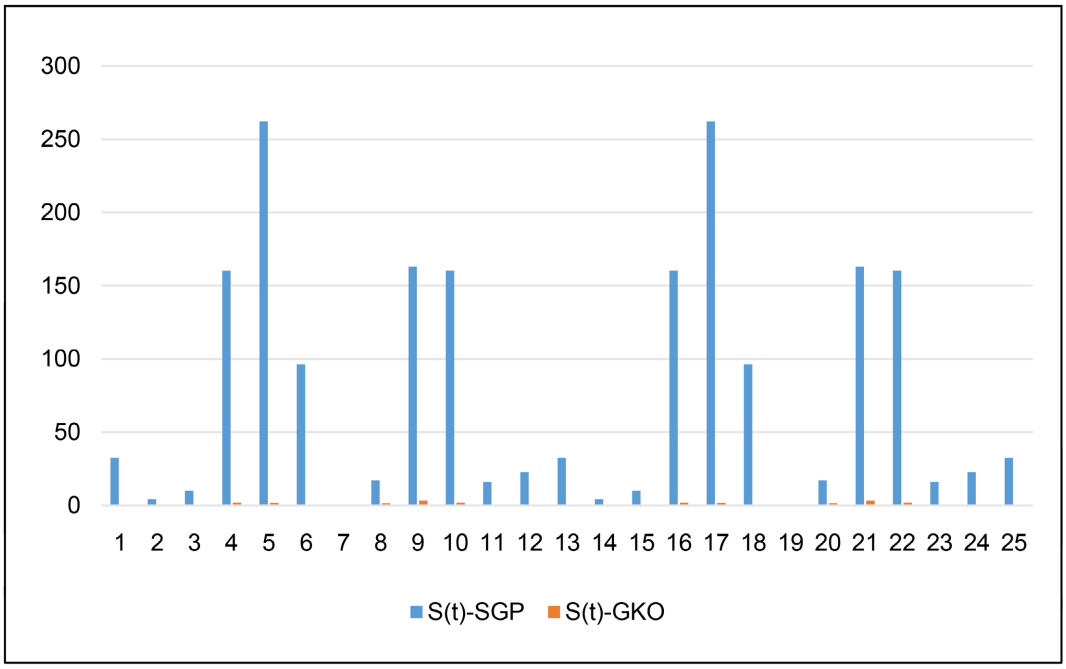

Figure 14. Diurnal variability of densification area in hectares (ha) Singapore (1.28˚N, 103.85˚E) and Guiriko (11.11˚N, 4.28˚W).

Thus, the greater amplitude of solar radiation power in W/m² K for Singapore than for Guiriko shows that cities near the equator receive the maximum amount of solar radiation for ionization production compared to cities further and further from the equator. However, if we consider the power density in W/m² given in the

variations in **Figure 13** above for the cities of Singapore and Guiriko (Bobo-Dioulasso), respectively, this is not the case, due to the distribution of solar radiation at the equator over a large area (**Figure 14** above). Indeed, the power density, or the proportion of power received by each point or city, increases at latitudes further and further from the equator, up to latitudes of 37˚ and 38˚ North and South, respectively [23]. This implies that the electron density n_e is increasingly reduced as one approaches the equator, which nevertheless exhibits an anomalous amplification of the current densities Sq. It can then be deduced that if this is the case, and by virtue of the relation ($J = n_e V_e$) that the cause of this increase is attributed to the speed of particle current and not to the existence of another additional current called equatorial electroject which would be specific to low latitude regions.

Since light is an electromagnetic wave, it propagates by carrying energy whose power density is given by the magnitude of the Poynting vector $\boldsymbol{\pi}$ and can be expressed as a function of the electric field vector $\boldsymbol{E}_0$ or magnetic field $\boldsymbol{B}_0$. It is given by one of the following expressions:

$$\mathrm{W}\cdot\mathrm{m}^{-2}\begin{cases}\left\|\langle\boldsymbol{\pi}\rangle\right\| = \dfrac{E_0^2}{2\mu_0\cdot C}\\ \left\|\langle\boldsymbol{\pi}\rangle\right\| = \dfrac{CB_0^2}{2\mu_0}\end{cases}\rightarrow\begin{cases}E_0 = \sqrt{2\mu_0\cdot C\cdot\left\|\langle\boldsymbol{\pi}\rangle\right\|}\\ B_0 = \sqrt{\dfrac{2\mu_0\left\|\langle\boldsymbol{\pi}\rangle\right\|}{C}}\end{cases} \tag{12}$$

If we consider $\left\|\langle\boldsymbol{\pi}\rangle\right\| = D_p$ From the previously calculated ionosphere, we find the value of the magnetic field or that of the electric field. Thus, the daily variation of the power density also affects the electric field, as shown in **Figure 14** above. At equatorial latitudes, the electric field will be weaker than at even more distant latitudes. It then follows, as a deduction, that due to the density ($J(t) = \sigma E$) very high ionospheric currents Sq at the equator mean that the electrical conductivity σ of the plasma is very high.

4.2. Toroidal Movement of the Ionization Densification Surface (EEJ/CEJ or REJ)

If the power density of the ionization densification surface has, on the one hand, confirmed the amplification of plasma conductivity at the equator and, on the other hand, led to the conclusion that the increase in the so-called anomalous Sq current density is due to an increase in plasma flow velocity, does the explanation attributed to the existence of the equatorial electrojet still hold true? Or should further clarification be considered?

If this hypothesis seems to be plausible, we think more of the effect of speed due to the very high production factor k at latitudes close to the equator (**Figure 15**). This speed would increase significantly whether the two plasma tributaries, one from the Northern Hemisphere and the other from the South, meet or not:

$$V_{M/R_1} = \sqrt{\dot{h}(t)^2 + \left[h(t)\dot{\varphi}\cos\lambda\right]^2} \tag{13}$$

At the equator $\cos\lambda = 1$ so:

$$V_{éq} = \sqrt{\dot{h}(t)^2 + \left[h(t)\dot{\varphi}\right]^2} > V_{\lambda} = \sqrt{\dot{h}(t)^2 + \left[h(t)\dot{\varphi}\cos\lambda\right]^2}$$

So, even if the $\dot{h}(t)$ and $h(t)$ are identical at all latitudes $V_{éq} > V_{\lambda}$ because $\cos\lambda \leq 1$. However, in the hypothesis of $\dot{h}(t)$ and $h(t)$ identical at all latitudes we could not observe an amplification of the density of currents Sq taking into account the very low electronic densities at latitudes very close to the equator $J(t) = n_e V(t)$. This is why we attribute the observed amplification of current densities to the production factor k which amplifies the $\dot{h}(t)$ and $h(t)$ towards the equator and consequently their speeds. So for a simplified example if we ignore the longitude effect, the k Singapore of 2511.54 and Bobo-Dioulasso of 285.72 the plasma flow speeds of Singapore each hour will be 8.79 times greater than those of Bobo-Dioulasso.

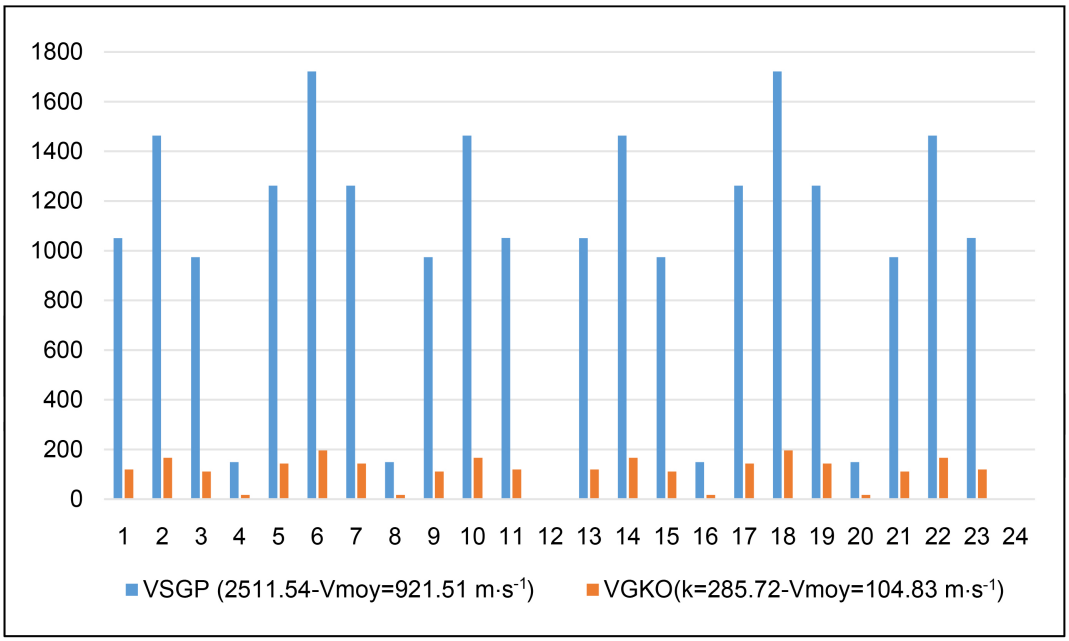

Figure 15. Densification surface velocity Singapore (1.28˚N, 103.85˚E) and Bobo-Dioulasso (11.11˚N, 4.28˚W).

These plasma streams do indeed circulate in the Southern Hemisphere in a clockwise direction, while those in the Northern Hemisphere circulate counter-clockwise. However, due to their twisting motions, reminiscent of the toroidal magnetic field of sunspots, the two streams, as shown in **Figure 16** and **Figure 17**, are not always oriented eastward. At times, while the Northern stream tends to orient itself eastward, the Southern stream tends to orient itself westward, and vice versa. At other times, the two streams do not even orient themselves eastward, but rather tend to orient themselves in a north-south direction; similarly, if one tends to orient itself northward, the other tends to orient itself southward, and vice versa.

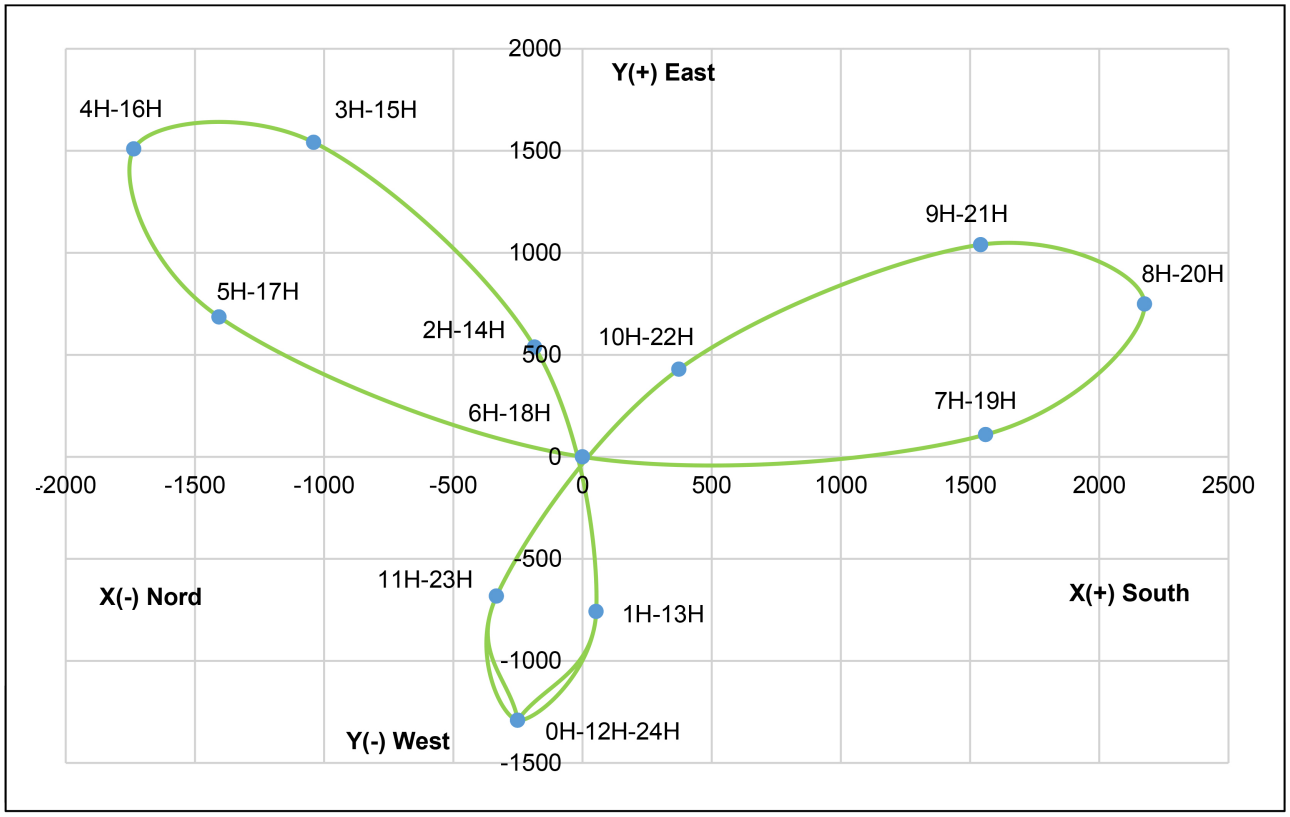

Figure 16. Movement of the ionospheric plasma flux—Singapore (Lat 1.28˚N, Long 103.85˚E).

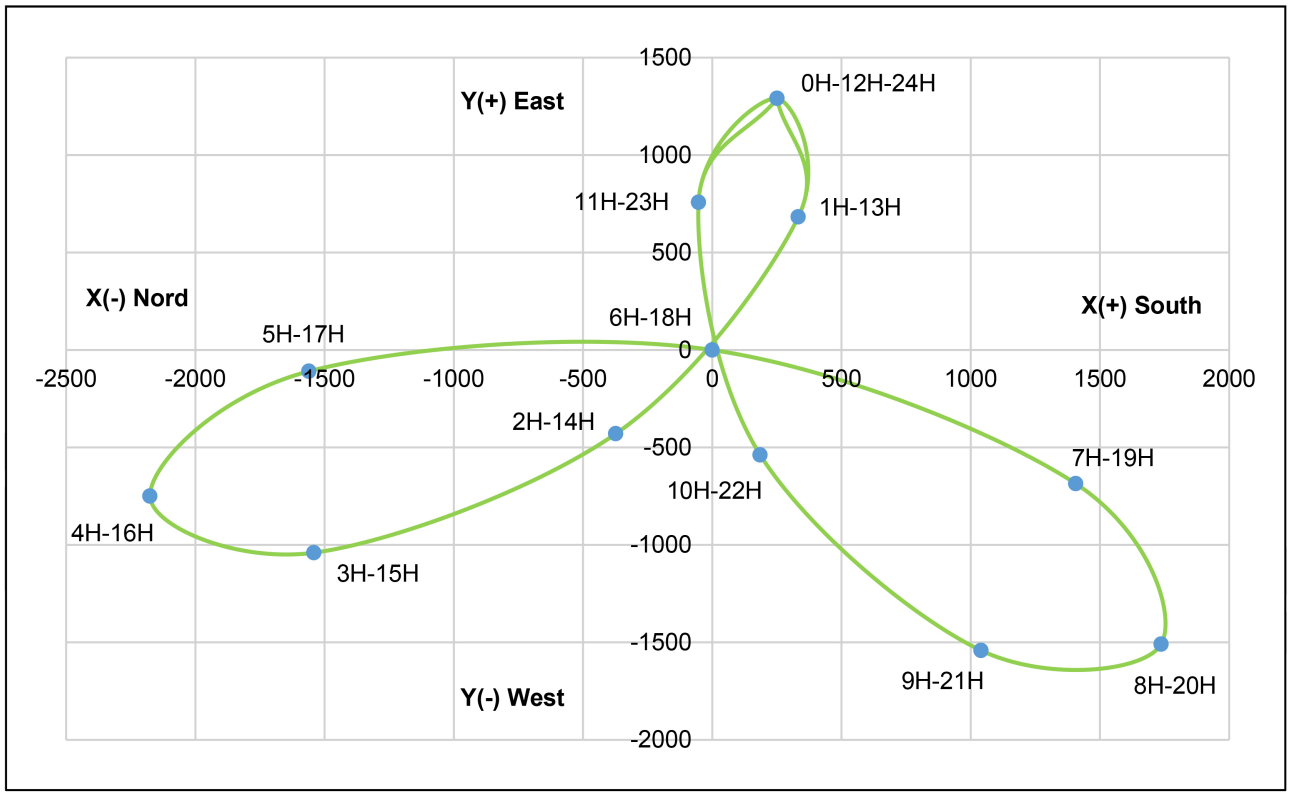

Figure 17. Movement of the ionospheric plasma flux (Lat 1.28˚S, Long 103.85˚E).

Thus 1) from 0 a.m. to 3 a.m. or from 12 p.m. to 3 p.m., a conjunction with a phase shift is observed. The plasma flow in the Northern hemisphere would tend to orient itself or align in the West-East direction, while that in the Southern hemisphere would tend to align in the East-West direction.

- From 1a) 0H to 3H and at the occurrence 3H, in the Northern Hemisphere we have production, the speed of the densification surface is therefore oriented downwards (**Figure 1**). We deduce that the movement of the whole is such that its component E_y is oriented from East to West (CEJ/REJ) from the fact that the potential E_z is counted positively. Thus we would obtain an asymmetry in current density Sq in favor of the Southern Hemisphere. This would result in an asymmetry in current density Sq in favour of the Southern hemisphere.
- 1b) From 12 p.m. to 3 p.m. and at the occurrence of 3 p.m., we observe a drift in the Northern hemisphere and therefore a drift speed oriented upwards (**Figure 2**). We then deduce that the movement of the entire plasma flow is such that its component E_y is positive and oriented from West to East (EEJ) due to the fact that the potential E_z is counted negatively. Thus we would obtain an asymmetry in current density Sq in favor of the Northern hemisphere. However, at 12 p.m. we observe production where the component E_y is negative and therefore oriented from East to West (CEJ/REJ) due to the fact that the drift speed is oriented downwards and therefore the potential E_z is counted positively.
- 1c) For the city of Bobo-Dioulasso, on the other hand, we observe EEJ electrojets at the hours of 3 a.m. and 12 p.m. and 3 p.m. CEJ counter electrojets.

2) Conversely, from 8 a.m. to 12 p.m. or from 8 p.m. to 12 a.m., the opposite effect is observed: the plasma flow moves from East to West in the Northern Hemisphere, and the Southern Hemisphere flows from West to East.

- However, 2a) from 8 a.m. to 12 p.m. at the occurrence of 9 a.m., we have production in the Northern hemisphere and therefore a production speed oriented downwards (**Figure 2**). We then deduce that the movement of the entire plasma flow is such that its component Ey is negative and therefore is oriented from East to West (CEJ/REJ) taking into account that the potential Ez is positive. Thus we would obtain an asymmetry in current density Sq in favor of the Northern hemisphere.
- 2b) On the other hand, from 8 p.m. to 12 p.m. at the occurrence of 21 p.m. and 24 p.m., we observe a vertical drift and therefore a positive speed in the Northern hemisphere (**Figure 2**). We then deduce that the movement of the entire plasma flow is such that its component E_y is positive and therefore oriented from West to East (EEJ) due to the fact that the potential E_z is counted negatively.
- 2c) For the city of Bobo-Dioulasso, on the other hand, we observe EEJ counter electrojets at the hours of 9 a.m. and CEJ counter electrojets at the hours of 9 p.m. and 24 p.m.

3) From 3 a.m. to 8 a.m. and from 3 p.m. to 8 p.m., there is a phase conjunction where a near-symmetry in current density (Sq) will tend to be observed between the Northern and Southern Hemispheres. Indeed, the two plasma flows would tend to orient themselves from North to South. Therefore, there would be neither

EEJ nor CEJ/REJ. This would be verified by Equation (10), as no magnetic declination angle allows its resolution.

4.3. Longitude Effect

Electrical conductivity, on the other hand, is obtained from the equality of current density as a function of velocity and current density as a function of the electric field. Thus $\sigma(t)$ will be given by the equation:

$$\sigma(t)=\frac{n_e}{E}V(t)=\frac{n_e}{\sqrt{2\mu_0\cdot C\cdot\|\langle\pi\rangle\|}}\sqrt{\dot{h}^2+(\omega\cdot h\cdot\cos\lambda)^2} \tag{14}$$

For example, we obtain the following graph (Figure 18) giving the spatio-temporal variability of the electrical conductivity from the maximum density NmE given by IRI 2020 on the date of 13/09/2025.

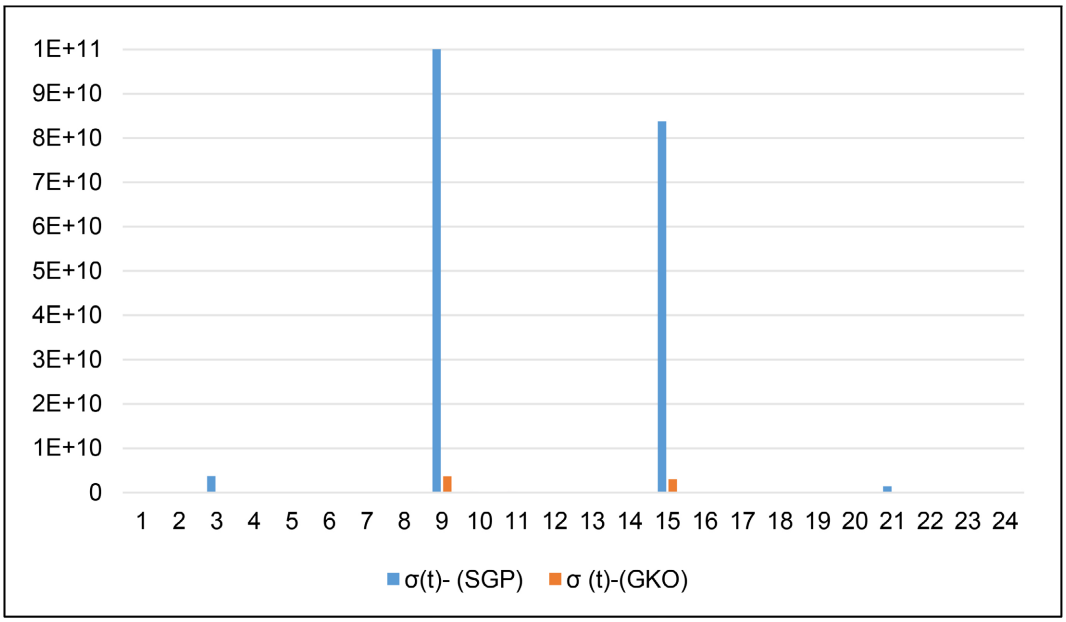

Figure 18. Electrical conductivity of the E layer obtained with NmE respectively—Singapore (σ-SGP, Lat 1.28˚N, Long 103.85˚E) and Bobo-Dioulasso (σ-GKO, Lat 11.11˚N, Long 4.28˚W).

Thus, the electrical conductivity as shown in Figure 19 below obtained is very high at certain times of the day: 3 a.m., 9 a.m., 3 p.m., 9 p.m. for the city of Singapore and 9 a.m. and 3 p.m. for the city of Bobo-Dioulasso.

However, for the same latitude λ and longitudes φ_1 and φ_2 different the conductivity rate will vary depending on the electron density $n_e(t)$, of the factor of production k and longitudes φ.

$$\begin{cases}\dfrac{\sigma(t)_{\lambda}\,\varphi_1}{\sigma(t)_{\lambda}\,\varphi_2}=\left(\dfrac{n_e(t)_{\lambda}\,\varphi_1}{n_e(t)_{\lambda}\,\varphi_2}\right)\times\left(\dfrac{k_{\lambda}\varphi_1}{k_{\lambda}\varphi_2}\right)^2\times\left(\dfrac{\cos\varphi_1}{\cos\varphi_2}\right)_{\lambda}\\ \varphi_1=\omega t-\varphi_{01};\varphi_2=\omega t-\varphi_{02}\end{cases} \tag{15}$$

For example, assuming identical electron densities $n_e(t)$ and production fac-

tors k, the variability of the conductivity rate at a given longitude relative to the Greenwich meridian will be of the form shown in Figure 20 below. Also, since the cosine function is even, the variability of the conductivities observed at eastern longitudes is identical to that at western longitudes. Thus, from observation, electrical conductivity varies throughout the day according to longitude. This variability is not uniform for a given hour across longitudes. For example, at 12:00 p.m., the observed electrical conductivities decrease from 0˚ to 90˚ and then increase from 90˚ to 180˚. However, at 8 a.m., electrical conductivities decrease from 0˚ to 30˚, increase from 30˚ to 110˚, then decrease again from 110˚ to 130˚ and increase from 130˚ to 180˚.

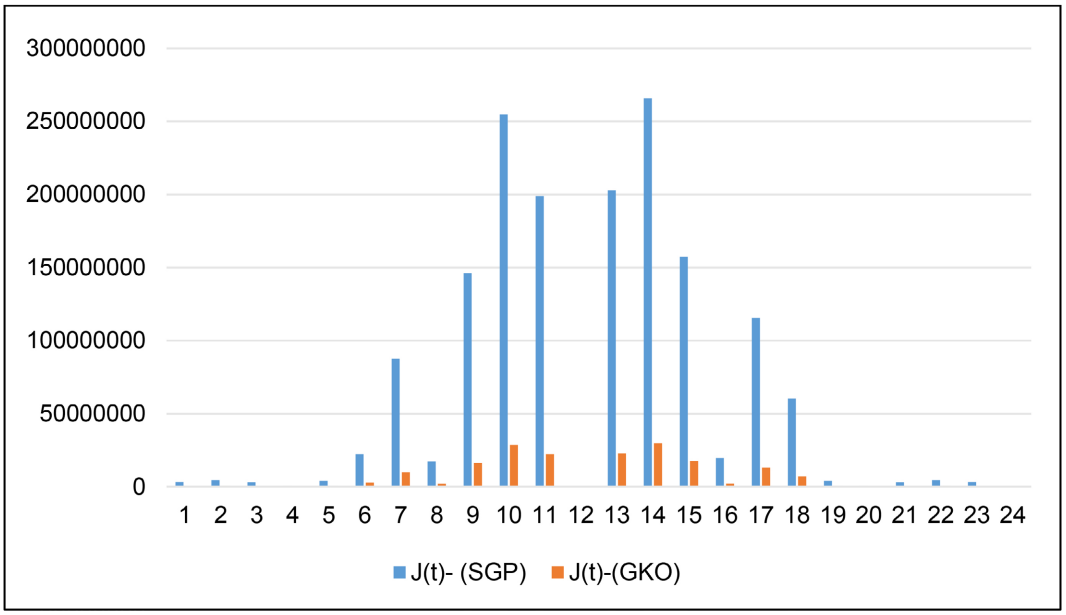

Figure 19. Electric current density of the E layer obtained with NmE respectively—Singapore (σ-SGP, Lat 1, 28˚N, Long 103.85˚E) and Bobo-Dioulasso (σ-GKO, Lat 11.11˚N, Long 4.28˚W).

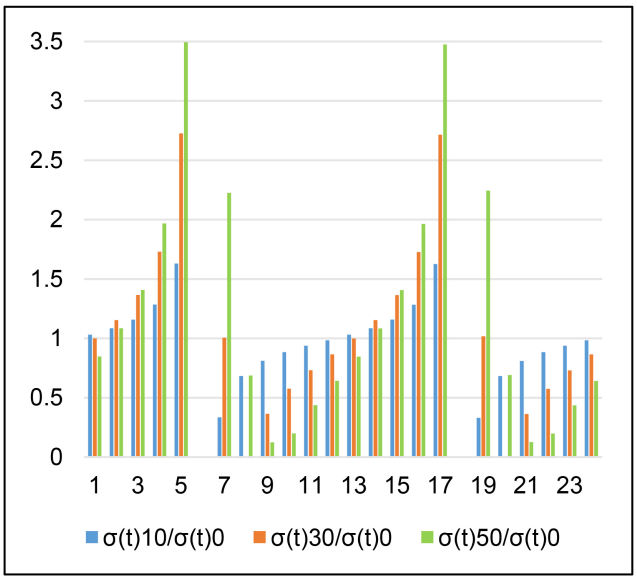

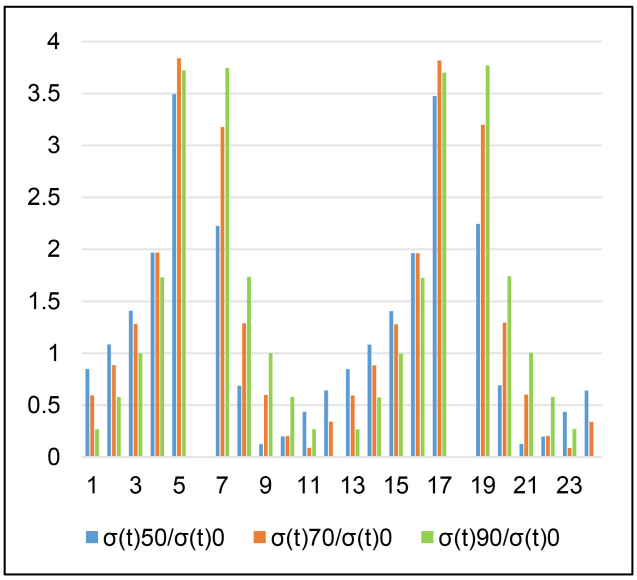

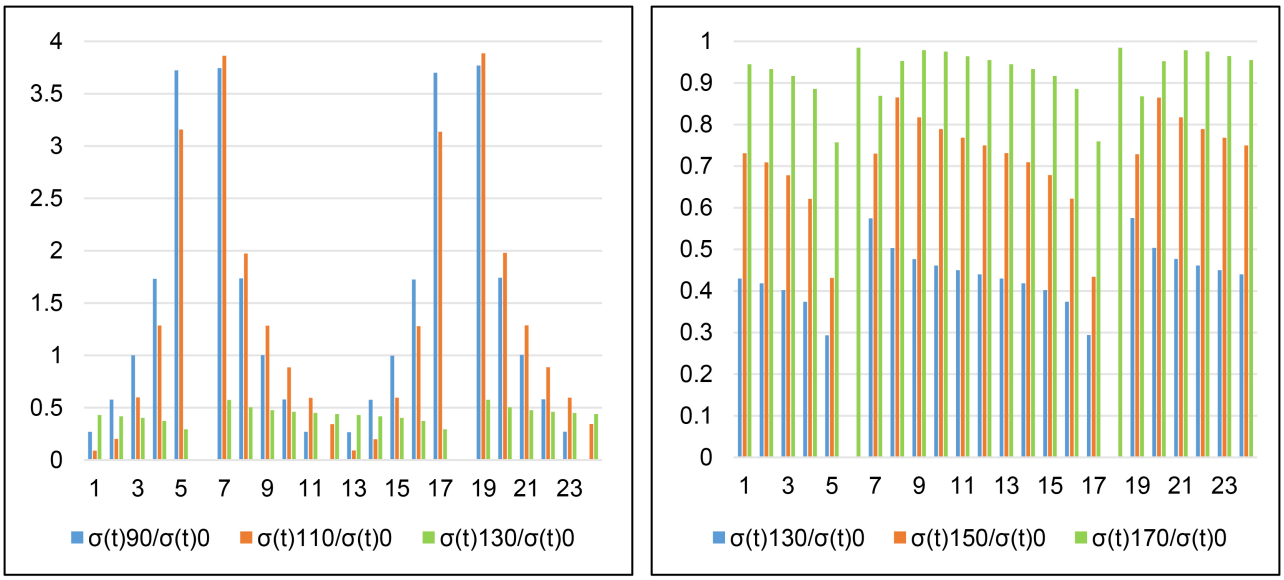

Figure 20. Conductivity rates of longitudes relative to the Greenwich meridian at longitudes 10˚, 50˚, 70˚, 90˚, 110˚, 130˚, 150˚, 170˚.

The electrical conductivity rates at 6 a.m. and 6 p.m. are not shown in the graph in Figure 19 but rather in Figure 21, given their very high values compared to the variability rates at other times. Specifically, the electrical conductivities are higher at 6 a.m. than at 6 p.m. and increase from 0˚ to 90˚ longitude, then generally decrease from 90˚ to 180˚ longitude.

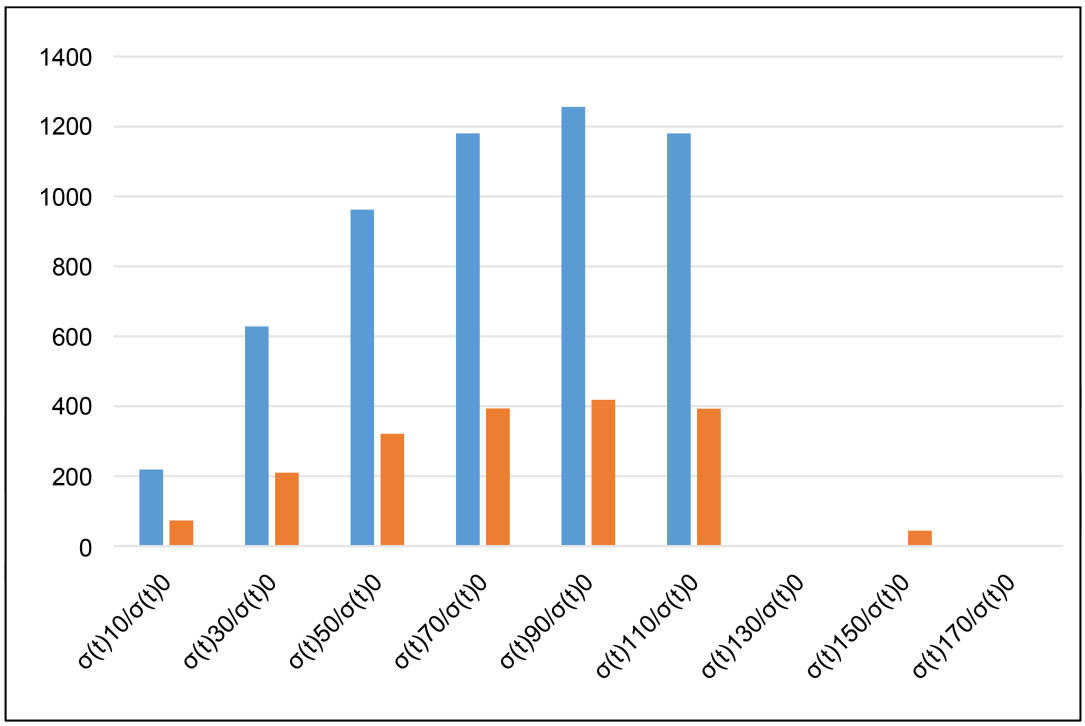

Figure 21. Conductivity rates of longitudes relative to the Greenwich meridian of longitudes 10˚, 50˚, 70˚, 90˚, 110˚, 130˚, 150˚, 170˚ at the hours of 6 a.m. (blue color) and 6 p.m. (orange color).

5. Synthesis

5.1. Similarities and Disagreements with Cowling's Conductivity for EEJ

$$\begin{cases} \boldsymbol{J}_{\text{Cowling}} = \left(\sigma_P + \dfrac{\sigma_H^2}{\sigma_P} \right) \boldsymbol{E}_{\text{EEJ}} = \sigma_C \boldsymbol{E}_{\text{EEJ}} \rightarrow \sigma_C = \sigma_P + \dfrac{\sigma_H^2}{\sigma_P} \\ \sigma(t) = \dfrac{n_e}{E} V(t) = \dfrac{n_e}{\sqrt{2\mu_0 \cdot C \cdot \left\| \langle \boldsymbol{\pi} \rangle \right\|}} \sqrt{\dot{h}^2 + \left(\omega \cdot h \cdot \cos\lambda \right)^2} \end{cases}$$

The proposed model offers an alternative explanation for the observed phenomenon of increased ionospheric current density at latitudes near the equator, coinciding with low electron density. The model relies on the power of solar radiation with an amplitude of $2k$, where k is a constant characteristic of the displacement of the ionization densification surface. Also called the ionization production factor k could be deduced at a given latitude using IRI 2020 data or by fitting with radar data (e.g., Jicamarca). The solar radiation power divided by the ionization densification area, which is proportional to k^2. This will give us the power density in watts per square meter, which will lead us to equate it to the magnitude of the Poything vector, since the light responsible for ionization is an electromagnetic wave. From this, the expressions for the temporal variability of both the electric and magnetic fields will be known for a given latitude and longitude. Thus, the first disagreement seems to be resolved. The origin of the electric field in the proposed model is not hypothetical, like the equatorial electrojet (EEJ) by which Cowling's electrical conductivity will be established. The proposed electric field is linked to light, surfaces, Latitudes and longitudes. The common point remains that both fields are weak at the equator. Also, the EEJ is horizontal, while the proposed electric field is neither horizontal nor vertical, and only its component E_y could model the EEJ. Such a model would depend on the ionization velocities V_{px}, V_{py}, V_{pz}, and the components of the magnetic field B_x, B_y, and B_z, and therefore on the inclination angles I and declination angles D. However, with the EEJ, V_{px} and V_{py} are assumed to be almost zero, and the magnetic field is oriented squarely towards the north, thus there is no B_y, and consequently, the inclination and declination angles are almost zero. Finally, the proposed conductivity is a formula integrating more than one parameter and describing the conductivity of ionospheric currents at any geographical location, while justifying the amplification of current densities at the equator.

5.2. Comparison of Calculated "Densification Surface" Trajectories with Established Ground-Based Magnetometer Data Models

The trajectory of the ionization densification surface at a given geographic location during the day is twisted, suggesting that the Sq currents are also twisted. Thus, by extension, a global view of the Earth would be similarly twisted, contrary to the observed concentric model. The common feature of the proposed model

with the data models is the direction of circulation: counterclockwise in the Northern Hemisphere and clockwise in the Southern Hemisphere. Also, the currents converge in phase at the equator in the established models, but not always in the proposed model. Only at the equator are the ionospheric currents amplified in the different models.

5.3. Importance

The study of the different ionospheric currents Sq, EEJ, and CEJ using the ionization densification surface was very satisfactory in several respects. 1) Based on knowledge of the position vector coordinates, a temporal and spatial evaluation of the ionization surface can be established. From this surface, the power density will be deduced, which will allow us, on the one hand, to justify the equatorial ionization anomaly and to determine the electric field through its equality with the magnitude of the Poynthing vector. On the other hand, knowledge of the electric field will justify the high ionospheric conductivity at latitudes very close to the equator. Finally, by observing the different positions of the densification surface, we can visualize the ionization trajectory or motion. 2) From the expression for velocity, it is shown, firstly, that the velocity is influenced by solar radiation, the Earth's rotation, and latitudinal position, and secondly, that this velocity is higher as one approaches the equator, thus explaining the high current density observed at these latitudes. 3) From knowledge of the trajectory or velocity vector, it is established that the ionization motion is clockwise in the Southern Hemisphere and counterclockwise in the Northern Hemisphere, and that they are not always in phase conjunction at the equator. 4) From knowledge of the magnetic field at the equator, and of the vertical drift or production velocity, the overall ionization motion is deduced, which sometimes reflects the electrojet or sometimes counter-electrojets with very precise time periods. From this overall motion, and from knowledge of the ionization motion in each hemisphere, the periods of symmetry and asymmetry will be determined. 5) This study offers a method, through the magnitude of the Poything vector and the ionospheric power density, for determining the magnitudes of the electric and magnetic fields and their various components.

$$\boldsymbol{E}\begin{cases} V_{pz}\geq 0\rightarrow E_x=\pm\left[-B\cdot V_{pz}\cdot\sin(D)\right] \text{ et } V_{pz}\leq 0\rightarrow E_x=\pm B\cdot V_{pz}\cdot\sin(D) \\ V_{pz}\geq 0\rightarrow E_y=\pm B\cdot V_{pz}\cdot\cos(D), V_{pz}\leq 0\rightarrow E_y=\pm\left[-B\cdot V_{pz}\cdot\cos(D)\right] \\ E_z=\pm\sqrt{E^2-V_{pz}^2B^2}, \end{cases}$$

$$\boldsymbol{B}\begin{cases} B_x=\dfrac{E_z}{V_{py}-V_{px}\cdot\tan(D)} \\ B_y=\dfrac{E_z}{V_{py}-V_{px}\cdot\tan(D)}\tan(D) \\ B_z=0 \end{cases} \begin{cases} \text{si } V_{pz}\geq 0\rightarrow E_z=-\sqrt{E^2-V_{pz}^2B^2} \\ \text{si } V_{pz}\leq 0\rightarrow E_z=\sqrt{E^2-V_{pz}^2B^2} \end{cases} \tag{16}$$

Finally, the declination angle will be determined starting from equality

" $E_y = -B_x V_{pz}$ " which leads to the solution of the equation:

$$B \cdot V_{px} \cdot \sin(D) - B \cdot V_{py} \cdot \cos(D) \pm E_z = 0$$

Thus, using calculation software like Excel and by varying the declination angles "D" from 0˚ to 90˚, the solution angles of the equation are identified, as well as the corresponding times or hours. Also, depending on the sign of E_y obtained by $-B_x V_{pz}$ one could also know if at these times it is an electrojet EEJ or a counter electrojet CEJ. 6) This study allows, through the expression of electrical conductivity, to know the value of this conductivity and, by induction, the electrical density at any geographical position and to know the effect of longitudes.

6. Conclusion

At the end of this study, structured around an introduction, methodology, results, discussion, and synthesis, the aim was to analyze ionospheric currents, specifically those of mid-latitudes (Solar Quiet) and low latitudes (EEJ and CEJ/REJ), and to draw conclusions regarding our perception. Thus, after presenting the Earth's magnetic field, Solar Quiet will be defined by some as the average of the five quietest days of the month, denoted Sq, and by others as the regular variation of a day of magnetic calm, denoted Solar Regulation Sr. Electrojets (EEJ) and reverse electrojets (CEJ/REJ), also called reverse electrojets, are currents whose definition is contested, as they are not universally accepted. For some, EEJ are horizontal currents flowing from west to east at latitudes centered on the equator. These currents will subsequently be called CEJ/REJ if they flow from East to West. For others, EEJ and CEJ/REJ are simply amplified Sq currents. Thus, after the introduction and following the methodology, which consisted of presenting the ionization densification surface on which the analysis is based, the essential steps for convincing the audience were presented, and the results section will allow for a visual observation of the temporal variation of certain parameters. These parameters include the ionization movement characteristic of Sq currents, which are counterclockwise in the Northern Hemisphere and clockwise in the Southern Hemisphere. They also include conductivity and electrical density. The discussion focused on three points: 1) The power density—electric field and electrical conductivity—through which the temporal variations of the magnetic and electric fields will be known via the Poything vector, which would allow us to show that if the conductivity of the currents Sq is very high at the equator and attributed by some to the Cowling effect, it is justified by the very weak electric field at the equator. 2) The toroidal motion of the ionization densification surface, through which the components of the electric field will be understood, that the ionospheric current at the equator is neither horizontal nor vertical, and through its component E_y, we could identify, by solving an equation that we will call the fundamental equation of EEJ/CEJ or REJ, on the one hand the times and on the other hand the magnetic declination angles corresponding to the electrojets and counter-electrojets, as well as their intensity. Thus, the hours 3 a.m., 9 a.m., and 12 p.m. correspond to CEJ/REJ, and 3 p.m., 9 p.m., and 12 a.m. to EEJ for the city of Singapore, and the

opposite for the city of Bobo-Dioulasso. 3) The longitude effect will be shown by demonstrating that while current density is very high at the equator and at increasingly distant latitudes, this is true for latitudes of the same or nearly the same longitude. Otherwise, for latitudes of different longitudes, at certain times of day, current densities at latitudes far from the equator are greater than those at latitudes near the equator. Finally, before reaching the conclusion, a section will be devoted to summarizing the study, highlighting the similarities and differences with Cowling's conductivity for EEJ, comparing the calculated "densification surface" trajectories with established ground-based magnetometer data models, and finally, discussing the study's significance. In short, we will retain from our perception and that of many others that EEJ/CEJ or REJ are simply amplified Sq currents and therefore of the same nature as Sq currents. Thus, after presenting the core of the work, future directions could include reflections on scintillations or auroral electrojets.

Conflicts of Interest

The authors declare no conflicts of interest regarding the publication of this paper.

References

[1] Yamazaki, Y. and Maute, A. (2017) Sq and EEJ—A Review on the Daily Variation of the Geomagnetic Field Caused by Ionospheric Dynamo Currents. In: *Space Sciences Series of ISSI*, Springer, 307-413.

[2] Chapman, S. and Bartels, J. (1940) Geomagnetism. Oxford University Press.

[3] Mayaud, P.N. (1965) Analyse morphologique de la variabilité jour à jour de la variation "régulière" Sr du champ magnétique terrestre, 1, le système de courants Cm (régions non polaires). *Annals of Geophysics*, **21**, 515.

[4] Graham, G. (1724) IV. An Account of Observations Made of the Variation of the Horizontal Needle at London, in the Latter Part of the Year 1772, and Beginning of 1723. *Philosophical Transactions of the Royal Society of London*, **33**, 96-107. https://doi.org/10.1098/rstl.1724.0020

[5] Graham, G. (1725) III. Observation of the Dipping Needle. Made at London, in the Beginning of the Year 1723. *Philosophical Transactions of the Royal Society of London*, **33**, 332-339. https://doi.org/10.1098/rstl.1724.0062

[6] Stewart, B. (1882) Hypothetical Views Regarding the Connection between the State of the Sun and Terrestrial Magnetism. In: *Encyclopedia Brittanica*, Vol. 16, 9th Edition, A&C Black, 181-184.

[7] Schuster, A. (1889) XV. The Diurnal Variation of Terrestrial Magnetism. *Philosophical Transactions of the Royal Society of London*. (*A.*), **180**, 467-518. https://doi.org/10.1098/rsta.1889.0015

[8] Schuster, A. (1908) IV. The Diurnal Variation of Terrestrial Magnetism. *Philosophical Transactions of the Royal Society of London. Series A, Containing Papers of a Mathematical or Physical Character*, **208**, 163-204. https://doi.org/10.1098/rsta.1908.0017

[9] Matsushita, S. (2007) Sq and L Current Systems in the Ionosphere. *Geophysical Journal of the Royal Astronomical Society*, **15**, 109-125. https://doi.org/10.1111/j.1365-246x.1968.tb05751.x

[10] Campbell, W.H. (1989) An Introduction to Quiet Daily Geomagnetic Fields. *Pure and Applied Geophysics*, **131**, 315-331. https://doi.org/10.1007/bf00876831

[11] Chapman, S. (1951) The Equatorial Electrojet as Detected from the Abnormal Electric Current Distribution above Huancayo, Peru, and Elsewhere. *Archiv für Meteorologie, Geophysik und Bioklimatologie Serie A*, **4**, 368-390. https://doi.org/10.1007/bf02246814

[12] Richmond, A.D. (1979) Ionospheric Wind Dynamo Theory: A Review. *Journal of Geomagnetism and Geoelectricity*, **31**, 287-310. https://doi.org/10.5636/jgg.31.287

[13] Richmond, A.D. (2013) The Ionospheric Wind Dynamo: Effects of Its Coupling with Different Atmospheric Regions. In: Johnson, R.M. and Killeen, T.L., Eds., *The Upper Mesosphere and Lower Thermosphere: A Review of Experiment and Theory*, American Geophysical Union, 49-65. https://doi.org/10.1029/gm087p0049

[14] Wagner, C.-U., Möhlmann, D., Schäfer, K., Mishin, V.M. and Matveev, M.I. (1980) Large-Scale Electric Fields and Currents and Related Geomagnetic Variations in the Quiet Plasmasphere. *Space Science Reviews*, **26**, 391-446. https://doi.org/10.1007/bf00217388

[15] Mayaud, P.N. (1980) Derivation, Meaning, and Use of Geomagnetic Indices. American Geophysical Union. https://doi.org/10.1029/gm022

[16] Love, J.J. and Gannon, J.L. (2009) Revised Dst and the Epicycles of Magnetic Disturbance: 1958-2007. *Annales Geophysicae*, **27**, 3101-3131. https://doi.org/10.5194/angeo-27-3101-2009

[17] Gjerloev, J.W. (2012) The SuperMAG Data Processing Technique. *Journal of Geophysical Research: Space Physics*, **117**, A09213. https://doi.org/10.1029/2012ja017683

[18] Svalgaard, L. and Cliver, E.W. (2007) Calibrating the Sunspot Number Using "the Magnetic Needle". *CAWSES News*, **4**, 6-8.

[19] Svalgaard, L. (2017) Erratum to: Reconstruction of Solar Extreme Ultraviolet Flux 1740-2015. *Solar Physics*, **292**, Article No. 20. https://doi.org/10.1007/s11207-016-1047-2

[20] Campbell, W.H. and Schiffmacher, E.R. (1988) Upper Mantle Electrical Conductivity for Seven Subcontinental Regions of the Earth. *Journal of Geomagnetism and Geoelectricity*, **40**, 1387-1406. https://doi.org/10.5636/jgg.40.1387

[21] Campbell, W.H., Barton, C.E., Chamalaun, F.H. and Welsh, W. (2014) Quiet-Day Ionospheric Currents and Their Application to Upper Mantle Conductivity in Australia. *Earth, Planets and Space*, **50**, 347-360. https://doi.org/10.1186/bf03352121

[22] Okeke, F.N. and Obiora, D.N. (2016) Application of Solar Quiet Day (sq) Current in Determining Mantle Electrical-Depth Conductivity Structure—A Review. *Journal of African Earth Sciences*, **114**, 54-62. https://doi.org/10.1016/j.jafrearsci.2015.11.015

[23] Segda, A.K., Kaboré, S., Gybre, A., Saidou, M. and Ouattara, F. (2025) Analysis and Estimation of the Vertical Drift Velocity from the Ionization Production Velocity in Correspondence with Radar Data from Jicamarca and IRI 2020. *Journal of Applied Mathematics and Physics*, **13**, 2674-2691. https://doi.org/10.4236/jamp.2025.138152

[24] Abdoul-kader, S., Allain, G.D. and Aristide, G. (2023) New Analysis of the Seasonal Variation of the Critical Frequencies Fof2 by a Proposed Formula of the Power of Solar Radiation. *International Journal of Geophysics*, **2023**, Article ID: 4405266. https://doi.org/10.1155/2023/4405266

[25] Yamazaki, Y. (2011) Study on Energy Transfer of Solar Radiation and Solar Wind into Equatorial Ionosphere. PhD Dissertation, Kyushu University.

[26] Ogbuehi, P.O., Onwumechilli, A. and Ifedili, S.O. (1967) The Equatorial Electrojet

and the World-Wide S Currents. *Journal of Atmospheric and Terrestrial Physics*, **29**, 149-160. https://doi.org/10.1016/0021-9169(67)90129-8

[27] Stening, R.J. (1995) What Drives the Equatorial Electrojet? *Journal of Atmospheric and Terrestrial Physics*, **57**, 1117-1128. https://doi.org/10.1016/0021-9169(94)00127-a

[28] Onwumechili, C.A. (1992) Study of the Return Current of the Equatorial Electrojet. *Journal of Geomagnetism and Geoelectricity*, **44**, 1-42. https://doi.org/10.5636/jgg.44.1

[29] Cowling, T.G. (1932) The Electrical Conductivity of an Ionised Gas in the Presence of a Magnetic Field. *Monthly Notices of the Royal Astronomical Society*, **93**, 90-97. https://doi.org/10.1093/mnras/93.1.90

[30] Grodji, F.O., Doumbia, V., Boka, K., Amory-Mazaudier, C., Cohen, Y. and Fleury, R. (2017) Estimating Some Parameters of the Equatorial Ionosphere Electrodynamics from Ionosonde Data in West Africa. *Advances in Space Research*, **59**, 311-325. https://doi.org/10.1016/j.asr.2016.09.004

[31] Forbes, J.M. and Lindzen, R.S. (1976) Atmospheric Solar Tides and Their Electrodynamic Effects—II. The Equatorial Electrojet. *Journal of Atmospheric and Terrestrial Physics*, **38**, 911-920. https://doi.org/10.1016/0021-9169(76)90074-x

[32] Takeda, M. and Maeda, H. (1981) Three-Dimensional Structure of Ionospheric Currents 2. Currents Caused by Semidiurnal Tidal Winds. *Journal of Geophysical Research*: *Space Physics*, **86**, 5861-5867. https://doi.org/10.1029/ja086ia07p05861

[33] Hanuise, C., Mazaudier, C., Vila, P., Blanc, M. and Crochet, M. (1983) Global Dynamo Simulation of Ionospheric Currents and Their Connection with the Equatorial Electrojet and Counter Electrojet: A Case Study. *Journal of Geophysical Research*: *Space Physics*, **88**, 253-270. https://doi.org/10.1029/ja088ia01p00253

[34] Stening, R.J., Meek, C.E. and Manson, A.H. (1996) Upper Atmosphere Wind Systems during Reverse Equatorial Electrojet Events. *Geophysical Research Letters*, **23**, 3243-3246. https://doi.org/10.1029/96gl02611

[35] Sridharan, S., Sathishkumar, S. and Gurubaran, S. (2009) Variabilities of Mesospheric Tides and Equatorial Electrojet Strength during Major Stratospheric Warming Events. *Annales Geophysicae*, **27**, 4125-4130. https://doi.org/10.5194/angeo-27-4125-2009

[36] Fejer, B.G., Olson, M.E., Chau, J.L., Stolle, C., Lühr, H., Goncharenko, L.P., *et al.* (2010) Lunar-Dependent Equatorial Ionospheric Electrodynamic Effects during Sudden Stratospheric Warmings. *Journal of Geophysical Research*: *Space Physics*, **115**, A00G03. https://doi.org/10.1029/2010ja015273

[37] Rastogi, R.G. and Patel, V.L. (1975) Effect of Interplanetary Magnetic Field on Ionosphere over the Magnetic Equator. *Proceedings of the Indian Academy of Sciences-Section A*, **82**, 121-141. https://doi.org/10.1007/bf03046722

[38] Rastogi, R.G. (1977) Geomagnetic Storms and Electric Fields in the Equatorial Ionosphere. *Nature*, **268**, 422-424. https://doi.org/10.1038/268422a0

[39] Rastogi, R.G. (1997) Midday Reversal of Equatorial Ionospheric Electric Field. *Annales Geophysicae*, **15**, 1309-1315. https://doi.org/10.1007/s00585-997-1309-2

[40] Kikuchi, T., Hashimoto, K.K., Kitamura, T.-I., Tachihara, H. and Fejer, B. (2003) Equatorial Counterelectrojets during Substorms. *Journal of Geophysical Research*: *Space Physics*, **108**, Article No. 1406. https://doi.org/10.1029/2003ja009915

[41] Kikuchi, T., Hashimoto, K.K. and Nozaki, K. (2008) Penetration of Magnetospheric Electric Fields to the Equator during a Geomagnetic Storm. *Journal of Geophysical Research*: *Space Physics*, **113**, A06214. https://doi.org/10.1029/2007ja012628

[42] Le Huy, M. and Amory-Mazaudier, C. (2005) Magnetic Signature of the Ionospheric Disturbance Dynamo at Equatorial Latitudes: "d_{dyn}". *Journal of Geophysical Research*: *Space Physics*, **110**, A10301. https://doi.org/10.1029/2004ja010578

[43] Yamazaki, Y., Kosch, M.J. and Emmert, J.T. (2015) Evidence for Stratospheric Sudden Warming Effects on the Upper Thermosphere Derived from Satellite Orbital Decay Data during 1967-2013. *Geophysical Research Letters*, **42**, 6180-6188. https://doi.org/10.1002/2015gl065395

[44] Blanc, M. and Richmond, A.D. (1980) The Ionospheric Disturbance Dynamo. *Journal of Geophysical Research*: *Space Physics*, **85**, 1669-1686. https://doi.org/10.1029/ja085ia04p01669

[45] Fuller-Rowell, T.J., Millward, G.H., Richmond, A.D. and Codrescu, M.V. (2002) Storm-Time Changes in the Upper Atmosphere at Low Latitudes. *Journal of Atmospheric and Solar-Terrestrial Physics*, **64**, 1383-1391. https://doi.org/10.1016/s1364-6826(02)00101-3

[46] Muralikrishna, P. and Kulkarni, V.H. (2008) Modeling the Meteoric Dust Effect on the Equatorial Electrojet. *Advances in Space Research*, **42**, 164-170. https://doi.org/10.1016/j.asr.2007.11.019

[47] Vassal, J. (1982) La variation du champ magnétique et ses relations avec l'électrojet équatorial au Sénégal oriental. *Annales de Géophysique*, **38**, 347-355.

[48] Dunford, E. (1967) The Relationship between the Ionospheric Equatorial Anomaly and the E-Region Current System. *Journal of Atmospheric and Terrestrial Physics*, **29**, 1489-1498. https://doi.org/10.1016/0021-9169(67)90102-x

Annex 1: $B_z = 0$

$$\boldsymbol{B}\begin{pmatrix} B_x \\ B_y \\ 0 \end{pmatrix} \wedge \boldsymbol{V}\begin{pmatrix} V_{px} \\ V_{py} \\ V_{pz} \end{pmatrix} = \begin{vmatrix} B_y & V_{py} \\ 0 & V_{pz} \\ B_x & V_{px} \\ B_y & V_{py} \end{vmatrix} = \begin{cases} E_x = B_y V_{pz} \\ E_y = -B_x V_{pz} \\ E_z = B_x V_{py} - B_y V_{px} \end{cases}$$

- **Component E_z**

$$\begin{cases} E_x^2 + E_y^2 = V_{pz}^2\left(B_x^2 + B_y^2\right) = V_{pz}^2 B^2 \\ E_x^2 + E_y^2 = E^2 - E_z^2 \\ E_z = \pm\sqrt{E^2 - V_{pz}^2 B^2} \end{cases} \rightarrow$$

- **Component E_y**

$$\begin{cases} -\tan D = -\dfrac{B_y}{B_x} = \dfrac{E_x}{E_y} \rightarrow E_x = -E_y \tan D \\ E_x^2 + E_y^2 = E_y^2\left(1 + \tan^2(D)\right) = \dfrac{E_y^2}{\cos^2(D)} \\ \dfrac{E_y^2}{\cos^2(D)} = V_{pz}^2 B^2 \rightarrow E_y = \pm\left|B \cdot V_{pz} \cdot \cos(D)\right| \rightarrow E_y = \pm\left|V_{pz}\right| \cdot B \cdot \cos(D) \end{cases}$$

$$\rightarrow \begin{cases} V_{pz} \geq 0 \rightarrow E_y = \pm B \cdot V_{pz} \cdot \cos(D) \\ V_{pz} \leq 0 \rightarrow E_y = \pm\left[-B \cdot V_{pz} \cdot \cdot \cos(D)\right] \end{cases}$$

- **Component E_x**

$$\begin{cases} E_x = -E_y \tan D \\ V_{pz} \geq 0 \rightarrow E_y = \pm B \cdot V_{pz} \cdot \cos(D) \rightarrow E_x = \pm\left[-B \cdot V_{pz} \cdot \sin(D)\right] \\ V_{pz} \leq 0 \rightarrow E_y = -B \cdot V_{pz} \cdot \cos(D) \rightarrow E_x = \pm B \cdot V_{pz} \cdot \sin(D) \end{cases}$$

- **Component B_x**

$$\begin{cases} E_z = \pm\sqrt{E^2 - V_{pz}^2 B^2} \rightarrow B_y = B_x \tan(D) \\ E_z = B_x V_{py} - B_y V_{px} \rightarrow E_z = B_x\left(V_{py} - V_{px} \cdot \tan(D)\right) \\ \dfrac{E_z}{V_{py} - V_{px} \cdot \tan(D)} = B_x \rightarrow B_x = \dfrac{E_z}{V_{py} - V_{px} \cdot \tan(D)} \end{cases}$$

- **Component B_y**

$$\rightarrow \begin{cases} B_y = \dfrac{E_z}{V_{py} - V_{px} \cdot \tan(D)} \tan(D) \\ B_y = \dfrac{E_z}{V_{py} \cos(D) - V_{px} \cdot \sin(D)} \sin(D) \end{cases}$$

- **The magnetic declination angle or fundamental equation of EEJ/CEJ**

$$\begin{cases} E_y = -B_x V_{pz} \to E_y = -\dfrac{E_z}{V_{py} - V_{px} \cdot \tan(D)} V_{pz} \\ V_{pz} \geq 0 \to E_y = \pm B \cdot V_{pz} \cdot \cos(D), V_{pz} \leq 0 \to E_y = \pm\left[-B \cdot V_{pz} \cdot \cos(D)\right] \\ \dfrac{E_z}{V_{py} - V_{px} \cdot \tan(D)} = \mp B \cdot \cos(D) \end{cases}$$

$$\begin{cases} \text{si } E_y = B \cdot V_{pz} \cdot \cos(D) \to V_{pz} \geq 0, V_{pz} \leq 0 \\ E_z = -B \cdot \cos(D)\left(V_{py} - V_{px} \cdot \tan(D)\right) \\ E_z = -B \cdot V_{py} \cdot \cos(D) + B \cdot V_{px} \cdot \sin(D) \end{cases}$$

$$\to B \cdot V_{px} \cdot \sin(D) - B \cdot V_{py} \cdot \cos(D) - E_z = 0$$

$$\begin{cases} \text{si } E_y = -B \cdot V_{pz} \cdot \cos(D) \to V_{pz} \geq 0, V_{pz} \leq 0 \\ E_z = B \cdot \cos(D)\left(V_{py} - V_{px} \cdot \tan(D)\right) \\ E_z = B \cdot V_{py} \cdot \cos(D) - B \cdot V_{px} \cdot \sin(D) \end{cases}$$

$$\to B \cdot V_{px} \cdot \sin(D) - B \cdot V_{py} \cdot \cos(D) + E_z = 0$$

As $E_z = \pm\sqrt{E^2 - V_{pz}^2 B^2}$ one could consider either one as the fundamental equation of EEJ/CEJ or REJ.

Annex 2: $B_z \neq 0$

$$\boldsymbol{B}\begin{pmatrix} B_x \\ B_y \\ B_z \end{pmatrix} \wedge \boldsymbol{V}\begin{pmatrix} V_{px} \\ V_{py} \\ V_{pz} \end{pmatrix} = \begin{vmatrix} B_y & V_{py} \\ B_z & V_{pz} \\ B_x & V_{px} \\ B_y & V_{py} \end{vmatrix} = \begin{cases} E_x = B_y V_{pz} - B_z V_{py} \\ E_y = B_z V_{px} - B_x V_{pz} \\ E_z = B_x V_{py} - B_y V_{px} \end{cases}$$

$$\begin{cases} E_x^2 = \left(B_y V_{pz}\right)^2 - 2\left(B_y V_{pz}\right)\left(B_z V_{py}\right) + \left(B_z V_{py}\right)^2 \\ E_y^2 = \left(B_z V_{px}\right)^2 - 2\left(B_z V_{px}\right)\left(B_x V_{pz}\right) + \left(B_x V_{pz}\right)^2 \\ E_z^2 = \left(B_x V_{py}\right)^2 - 2\left(B_x V_{py}\right)\left(B_y V_{px}\right) + \left(B_y V_{px}\right)^2 \end{cases}$$

$$\begin{cases} E_x^2 + E_y^2 = \left(V_{pz}\right)^2\left[\left(B_y\right)^2 + \left(B_x\right)^2\right] + \left(B_z V_{py}\right)^2 + \left(B_z V_{px}\right)^2 \\ \qquad\qquad - 2\left(V_{pz} \cdot V_{py}\right)\left(B_z \cdot B_y\right) - 2\left(V_{pz} \cdot V_{px}\right)\left(B_z \cdot B_x\right) \\ E_x^2 + E_y^2 = E^2 - E_z^2 \to E_z^2 = E^2 - \left(E_x^2 + E_y^2\right) \\ \left(B_x V_{py}\right)^2 - 2\left(B_x V_{py}\right)\left(B_y V_{px}\right) + \left(B_y V_{px}\right)^2 + \left(E_x^2 + E_y^2\right) - E^2 = 0 \end{cases}$$

$$\begin{cases} \left(B_x V_{py}\right)^2 - 2\left(B_x V_{py}\right)\left(B_y V_{px}\right) + \left(E_x^2 + E_y^2\right) - E^2 = 0 \\ \left(V_{pz}\right)^2\left[\left(B_y\right)^2 + \left(B_x\right)^2\right] + \left(V_{py}\right)^2\left[\left(B_z\right)^2 + \left(B_x\right)^2\right] + \left(V_{px}\right)^2\left[\left(B_z\right)^2 + \left(B_y\right)^2\right] \\ -2\left(V_{pz} \cdot V_{py}\right)\left(B_z \cdot B_y\right) - 2\left(V_{pz} \cdot V_{px}\right)\left(B_z \cdot B_x\right) - 2\left(V_{py} \cdot V_{px}\right)\left(B_y \cdot B_x\right) - E^2 = 0 \end{cases}$$

$$\begin{cases} B_x = B\cdot\cos I\cdot\cos D \\ B_y = B\cdot\sin I\cdot\cos D \\ B_z = B\cdot\sin I \end{cases} \rightarrow \begin{cases} \left[\left(B_y\right)^2+\left(B_x\right)^2\right] = B^2\cdot\left(\cos D\right)^2 \\ \left[\left(B_z\right)^2+\left(B_x\right)^2\right] = B^2\cdot\left[\left(\sin I\right)^2+\left(\cos I\cdot\cos D\right)^2\right] \\ \left[\left(B_z\right)^2+\left(B_y\right)^2\right] = B^2\cdot\left[\left(\sin I\right)^2+\left(\sin I\cdot\cos D\right)^2\right] \end{cases}$$

$$\begin{cases} \left(V_{pz}\right)^2\cdot B^2\cdot\left(\cos D\right)^2+\left(V_{py}\right)^2 B^2\cdot\left[\left(\sin I\right)^2+\left(\cos I\cdot\cos D\right)^2\right]+\left(V_{px}\right)^2 B^2\cdot\left[\left(\sin I\right)^2+\left(\sin I\cdot\cos D\right)^2\right] \\ -2\left(V_{pz}\cdot V_{py}\right)B^2\cdot\left(\sin I\right)^2\cdot\cos D-\left(V_{pz}\cdot V_{px}\right)B^2\cdot\sin 2I\cdot\cos D-\left(V_{py}\cdot V_{px}\right)B^2\cdot\sin 2I\cdot\left(\cos D\right)^2-E^2=0 \\ B^2\cdot\left[\left(V_{pz}\right)^2\cdot\left(\cos D\right)^2+\left(V_{py}\right)^2\cdot\left[\left(\sin I\right)^2+\left(\cos I\cdot\cos D\right)^2\right]+\left(V_{px}\right)^2\cdot\left[\left(\sin I\right)^2+\left(\sin I\cdot\cos D\right)^2\right]\right] \\ B^2\cdot\left[-2\left(V_{pz}\cdot V_{py}\right)\cdot\left(\sin I\right)^2\cdot\cos D-\left(V_{pz}\cdot V_{px}\right)\cdot\sin 2I\cdot\cos D-\left(V_{py}\cdot -V_{px}\right)\cdot\sin 2I\cdot\left(\cos D\right)^2\right]-E^2=0 \end{cases}$$

Thus, the EEJ and CEJ/REJ are known through the sign of E_y given by the equation:

$$E_y = B\cdot\left[V_{px}\cdot\left(\sin I\right)-V_{pz}\cdot\left(\cos I\cdot\cos D\right)\right]$$

However, there is one condition:

$$\begin{cases} B^2\cdot\left[\left(V_{pz}\right)^2\cdot\left(\cos I\right)^2+\left(V_{py}\right)^2\cdot\left[\left(\sin I\right)^2+\left(\cos I\cdot\cos D\right)^2\right]+\left(V_{px}\right)^2\cdot\left[\left(\sin I\right)^2+\left(\sin I\cdot\cos D\right)^2\right]\right] \\ B^2\cdot\left[-2\left(V_{pz}\cdot V_{py}\right)\cdot\left(\sin I\right)^2\cdot\cos D-\left(V_{pz}\cdot V_{px}\right)\cdot\sin 2I\cdot\cos D-\left(V_{py}\cdot V_{px}\right)\cdot\sin 2I\cdot\left(\cos D\right)^2\right]-E^2=0 \end{cases}$$

Note: Some use the notations "F or…" and "H or…" to denote respectively the total intensity of the magnetic field and that of its horizontal component.